Supporting Information for:

A Novel Yttrium-based Metal-Organic Framework for the Efficient Solvent-Free Catalytic Synthesis of Cyanohydrin Silyl Ethers.

Estitxu Echenique-Errandonea,[†,1] Juana M. Pérez,[‡,1] Sara Rojas,[§] Javier Cepeda,[†] José M. Seco,[†] Ignacio Fernández*,[‡] and Antonio Rodríguez-Diéguez*,[§]

[†] Departamento de Química Aplicada, Facultad de Química, Universidad del País Vasco UPV/EHU, Paseo Manuel Lardizabal, Nº 3, 20018, Donostia-San Sebastián, Spain.

[‡] Department of Chemistry and Physics, Research Centre CIAIMBITAL, University of Almería, Ctra. Sacramento, s/n, 04120, Almería, Spain. Email: ifernan@ual.es

[§] Departamento de Química Inorgánica, Facultad de Ciencias, Universidad de Granada, Av. Fuentenueva S/N, 18071 Granada, Spain. Email: antonio5@ugr.es

Table of Contents:

1. General experimental information 3
2. General procedures 5
3. Crystallographic data 7
4. Selected bond lengths and angles data 8
5. Experimental PXRD 9
6. FTIR analysis of Ligand and Catalyst 10
7. Continuous Shape Measurements 11
8. Thermal analysis 12
9. Additional views of the structure 13
10. Luminescence properties 14
11. Optimization of the reaction conditions 15
12. Characterization Data of Products 16
13. NMR Spectra of New Compounds 20
14. IR Spectra of New Compounds 25
15. Catalyst Recyclability 27
16. Leaching test 28
17. View of possible active sites in pores 29
18. Proposed mechanisms for the MOF-catalyzed cyanosilylation reaction 30
19. Results obtained with different lanthanides MOF catalysts. 32
20. References 34

1. General experimental information

All experiments involving moisture-sensitive compounds were performed under an inert atmosphere of N_2 using standard techniques. Unless otherwise indicated, reagents and substrates were purchased from commercial sources and used as received. Solvents not required to be dry were purchased as technical grade and used as received. Conversion values relative to the limiting reagent were calculated from the ^{1}H NMR spectra of the reaction crudes. Isolated products were obtained after centrifugation (8000 rpm, 3 min) and washed with dichloromethane (2 x 0.5 mL) in order to remove the catalyst or column chromatography in silica gel using hexane as eluent.

NMR measurements: NMR spectra were measured in a Bruker Avance III 300 spectrometer equipped with a direct double SmartProbe BBFO ^{1}H/BB(^{19}F) probe. Chemical shifts are reported in parts per million (ppm) relative to residual solvent peak ($CDCl_3$, ^{1}H: 7.26 ppm; ^{13}C: 77.16 ppm). Coupling constants are reported in Hertz. Multiplicity is reported with the usual abbreviations (s: singlet, bs: broad singlet, d: doublet, dd: doublet of doublets, ddd: doublet of doublet of doublets, t: triplet, td: triplet of doublets, q: quartet, dq: doublet of quartet, p: pentet, sex: sextet, hept: heptet, m: multiplet).

IR (ATR) spectra of products **3** were recorded in a FT-IR Bruker Alpha spectrophotometer whereas IR spectra of Ligand and Compound **1** were recorded on a Nicolet 6700 FTIR spectrophotometer (Thermo Phisher Scientific, TX, USA) with samples as KBr disks.

Elemental analyses (EA) of the new synthesized cyanosilyl ethers **3** were performed on an Elementar vario EL cube in the CHN mode.

Photoluminescence measurements. Photoluminescence (PL) measurements were carried out on crystalline samples at room temperature using a Varian Cary-Eclipse fluorescence spectrofluorometer equipped with a Xe discharge lamp (peak power equivalent to 75 kW), Czerny–Turner monochromators, and an R-928 photomultiplier tube. For the fluorescence measurements, the photomultiplier detector voltage was fixed at 600 V, and the excitation and emission slits were set at 5 and 5 nm, respectively.

Thermogravimetric analysis (TG/DTA) were performed on a TG-Q500 TA Instruments thermal analyser from room temperature to 800 °C under a synthetic air atmosphere (79% N_2/21% O_2) at a heating rate of 10 °C min^{-1}.

X-ray Diffraction Data Collection and Structure Determination. Single-crystal diffraction data were collected at 100(2) K on a Bruker X8 APEX II and Bruker D8 Venture with a Photon detector equipped with graphite monochromated MoKα radiation (λ = 0.71073 Å). The data reduction was performed with the APEX2 software[1] and corrected for absorption using SADABS.[2] These structures were solved by direct methods using the SHELXT program[3] and refined by full-matrix least-squares of F2 including all reflections with SHELXL-2018/3 program.[4] All calculations for these structures were performed using the WINGX crystallographic software package.[5]

Powder X-ray diffractions (XRPD) patterns were collected on a Philips X'PERT powder diffractometer with Cu Kα radiation (λ = 1.5418 Å) over the range of $5 < 2\theta < 50°$ with a step size of 0.02° and an acquisition time of 2.5 s per step at 25 °C. Indexation of the diffraction profiles were carried out using the FULLPROF program,[6] on the basis of the space group and cell parameters found for isostructural compounds by single crystal X-ray diffraction.

2. General procedures

General procedure for the synthesis of Y-MOF (1): 10 mg (0.0625 mmol) of 3-amino-4-hydroxybenzoic acid (HL) organic linker was dissolved in 0.5 mL of DMF containing 10 µL of Et_3N (0.072mmol). $Y(NO_3)_2 \cdot 6H_2O$ (17 mg, 0.0434 mmol) was dissolved into a 0.5 mL of distilled water in a separate vial. Once dissolved, 0.5mL of H_2O was added to the ligand solution and 0.5 mL of DMF to the metal solution. Metal solution was added dropwise to the ligand solution keeping magnetic stirring. The resulting yellow solution was poured into a screw-capped vial (6 mL) and introduced to the oven at 100 °C for 2 hours to give rise hexagonal shaped single crystals. Single-crystal X-ray structure determination, elemental analysis (EA) and TGA confirm the general formula $[Y_5L_6(OH)_3(DMF)_3] \cdot 5H_2O$. EA for $C_{51}H_{64}N_9O_{29}Y_5$ (1711.64 g mol^{-1}). Calcd: C, 35.79; H, 3.77; N, 7.36. Found: C, 35.69; H, 3.71; N, 7.40.

General procedure for the cyanosilylation reaction: In a 1 ml vial with a septum screw capped equipped with a stirring bar, Y-MOF catalyst (2.3 mg, 0.5 mol%) was weighed Subsequently, the corresponding amount of carbonylic compound **2** (0.25 mmol) was added followed by trimethylsilyl cyanide (TMSCN) (34 µL, 0.275 mmol, 1.1 equiv.) and the reaction was stirred under inert N_2 atmosphere at room temperature during the corresponding time. Once the reaction was finished the catalyst was removed by centrifugation (8000 rpm, 3 min) and washed with DCM (2 x 0.5 mL) obtaining the corresponding pure product **3** after removal of the solvent with rotary evaporator. When not fully conversion was reached the product was purified by column chromatography using hexane as eluent.

General procedure for the gram scale reaction: In a 3 mL vial equipped with septum and stirring bar, it was weigh Y-MOF catalyst (46.52 mg, 0.5 mol%). Then, it was added benzaldehyde **2a** (507 µL, 5 mmol) followed by TMSCN (688 µL, 5.5 mmol, 1.1 equiv) and the reaction was stirred under inert N_2 atmosphere at room temperature during 5 hours. Once the reaction was finished the catalyst was removed by centrifugation (8000 rpm, 3 min) and washed with DCM (2 x 2 mL) obtaining the corresponding pure product **3a** after removal of the solvent with rotary evaporator with 86% isolated yield (877.8 mg).

Quantitative NMR acquisition parameters. ^1H NMR determination of product conversion was carried out by comparing signals arising from both CH of aldehyde **2** and cyanosilylated product **3**. The standard acquisition parameters were one-dimensional pulse sequence which includes a 30º flip angle (Bruker zg30), recycle time (D1 = 30 s), time domain (TD = 27k),

number of scans (NS = 32), acquisition time (AQ = 2.05 s), transmitter (frequency) offset (O1P = 6.0 ppm), and spectral width (SW = 22.0 ppm).

3. Crystallographic data

Table S1. Crystallographic data and structure refinement details of compound **1**.

Compound	**1**
Formula	$C_{51}H_{54}N_9O_{24}Y_5$
M_r	1711.63
Crystal system	hexagonal
Space group (no.)	*$P6_3/m$ (176)*
a(Å)	14.730(3)
b(Å)	14.730
c(Å)	17.616(5)
α(°)	90
β(°)	90
γ(°)	120
V(Å^3)	3310.1(17)
Z	2
ρ_{calc}g/cm^3	1.627
μ/mm^{-1}	4.415
F(000)	1620.0
Crystal size/mm^3	0.660 × 0.164 × 0.090
Radiation	MoKα (λ = 0.71073)
2Θ range for data collection/°	4.624 to 46.716
Index ranges	$-16 \leq h \leq 16$, $-16 \leq k \leq 16$, $-19 \leq l \leq 19$
Reflections collected	12689
Independent reflections	1674 [R_{int} = 0.0937, R_{sigma} = 0.0934]
Data/restraints/parameters	1672/24/145
Goodness-of-fit on F^2	1.087
Final R indexes [I>=2σ (I)]	R_1 = 0.0473, wR_2 = 0.1326
Final R indexes [all data]	R_1 = 0.0808, wR_2 = 0.1473
Largest diff. peak/hole / e Å^{-3}	1.16/-0.87

4. Selected bond lengths and angles data

Table S2. Table of the selected bond lengths (Å) and angles (°) for compound **1**.

Complex		1
Y1	O3	2.536(5)
Y1	N1	2.517(6)
Y1	O1H	2.349(4)
Y2	O1	2.425(5)
Y2	O2	2.396(5)
Y2	O3	2.349(5)
Y2	O1D	2.305(7)
Y2	O1H	2.348(6)

Complex			1		
N1	Y1	N1	81.5(2)		
N1	Y1	O3	64.60(17)	69.44(18)	137.62(19)
O1	Y2	O1	78.4(3)		
O1D	Y2	O1H	136.7(3)		
O1D	Y2	O3	81.1(2)		
O1D	Y2	O2	133.58(17)		
O1D	Y2	O1	82.5(2)		
O1H	Y1	O1H	71.50(18)		
O1H	Y1	N1	88.96(19)	132.1(2)	143.3(2)
O1H	Y1	O3	68.09(18)	74.49(19)	133.41(16)
O1H	Y1	Y1	42.43(11)		
O1H	Y2	O3	71.35(15)		
O1H	Y2	O2	75.35(18)		
O1H	Y2	O1	128.22(16)		
O2	Y2	O2	77.7(3)		
O2	Y2	O1	54.29(18)	102.08(19)	
O3	Y1	O3	119.956(9)		
O3	Y2	O3	99.1(2)		
O3	Y2	O2	81.82(18)	136.01(11)	
O3	Y2	O1	88.86(18)		
Y2	O3	Y1	107.03(17)	144.31(18)	
Y2	O1H	Y1	113.5(2)	160.43(18)	

5. Experimental PXRD

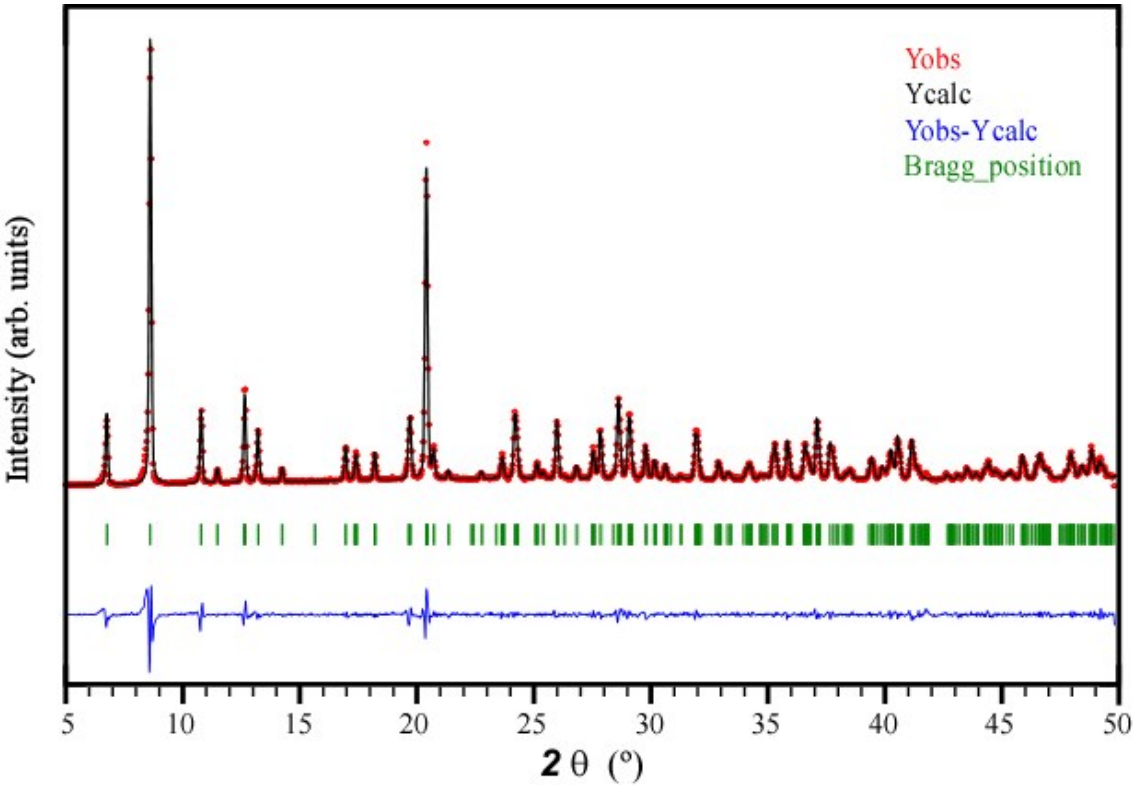

Figure S1. Figure of the pattern matching analysis and experimental PXRD for complex **1**.

6. FTIR analysis of Ligand and Catalyst

FTIR spectra of compound **1** exhibit a narrow peak at around 3671 cm^{-1} attributed to the N–H stretching vibration of the amine group of 3-amino-4-hydroxbenzoate ligand. Additionally, it shows a broad and intense band around 3424 cm^{-1} that corresponds to the vibration of the O–H bond of free ligand, followed by weak bands between 3245 and 2929 cm^{-1} corresponding to the C–H vibrations of the aromatic ring of the 3-amino-4-hydroxybenzoate ligand. The intense vibrations in the 1662–1433cm^{-1} region are attributed to both the asymmetric stretching vibrations of the carboxylate groups and the aromatic C–C and C–N bonds, while the symmetric stretching vibrations of the carboxylate groups appear in the lower range of 1399–1287 cm^{-1}. At lower frequencies, the remaining bands are attributed to the distortions originated in the aromatic ring and the carboxylate groups of the ligands. The vibration bands of the M–O and M–N bonds are observed below 662 cm^{-1}. Nevertheless, there are some clear differences according to the ligand and coordination mode, in particular those involving the vibrations of the carboxylate groups. Concerning the spectra of compounds **1**, they show typical vibration bands (a broad band centred at 1662 cm^{-1} plus a narrower band at 1600 cm^{-1}) assigned to the asymmetric vibrations of carboxylate moieties establishing the bis-chelating mode of the ligand.

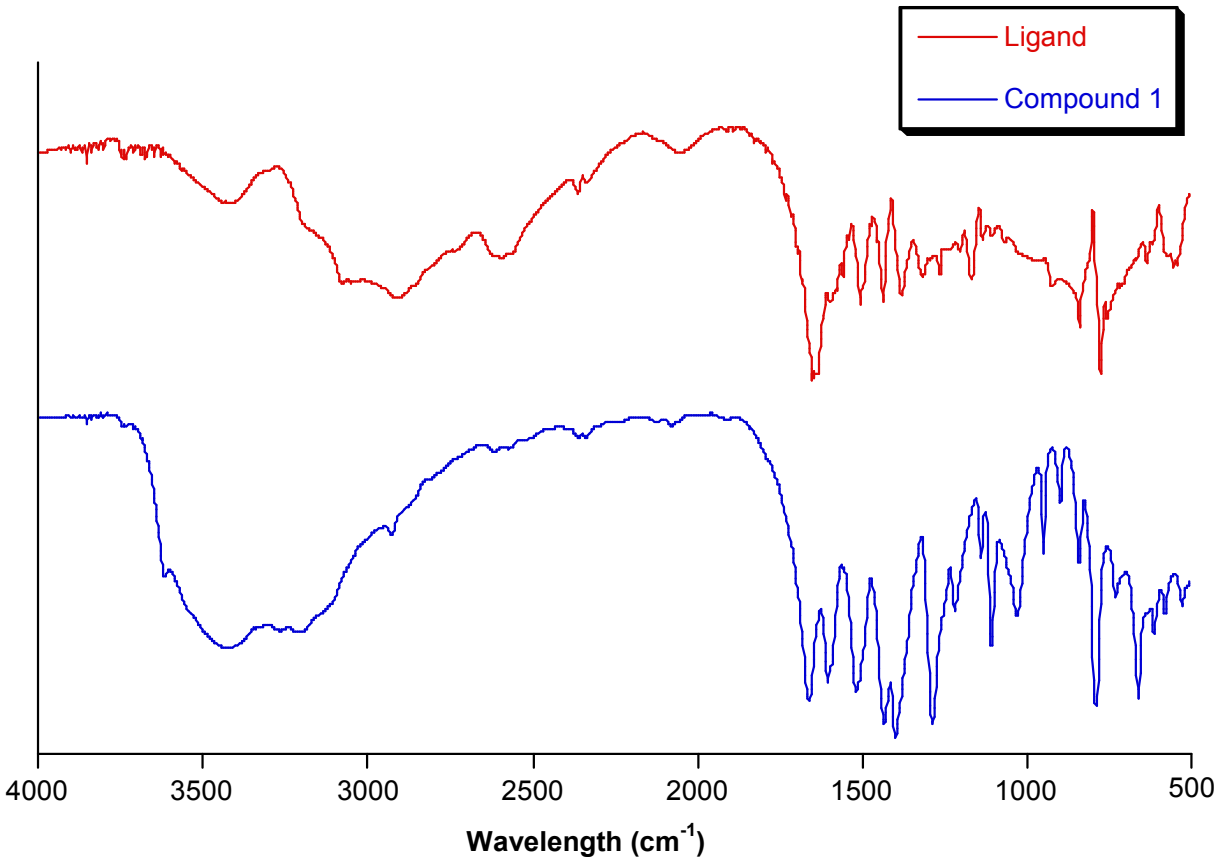

Figure S2. Figure of the infrared spectra of the ligand and compound **1**.

7. Continuous Shape Measurements

Table S3. Table of the continuous Shape Measurements for the LnN_3O_6 coordination environment.

EP-9	1 D9h	Enneagon
OPY-9	2 C8v	Octagonal pyramid
HBPY-9	3 D7h	Heptagonal bipyramid
JTC-9	4 C3v	Johnson triangular cupola J3
JCCU-9	5 C4v	Capped cube J8
CCU-9	6 C4v	Spherical-relaxed capped cube
JCSAPR-9	7 C4v	Capped square antiprism J10
CSAPR-9	8 C4v	Spherical capped square antiprism
JTCTPR-9	9 D3h	Tricapped trigonal prism J51
TCTPR-9	10 D3h	Spherical tricapped trigonal prism
JTDIC-9	11 C3v	Tridiminished icosahedron J63
HH-9	12 C2v	Hula-hoop
MFF-9	13 Cs	Muffin

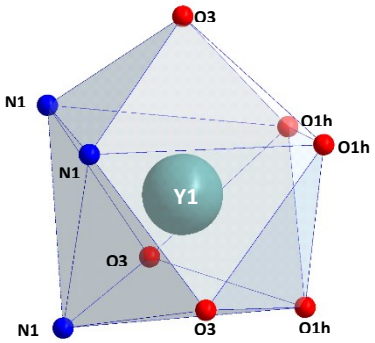

Complex	JCSAPR-9	CSAPR-9	JTCTPR-9	TCTPR-9	MFF-9
Y1	2.372	1.493	1.855	**0.829**	2.180

Table S4. Table of the continuous Shape Measurements for the LnO_8 coordination environment.

OP-8	1 D8h	Octagon
HPY-8	2 C7v	Heptagonal pyramid
HBPY-8	3 D6h	Hexagonal bipyramid
CU-8	4 Oh	Cube
SAPR-8	5 D4d	Square antiprism
TDD-8	6 D2d	Triangular dodecahedron
JGBF-8	7 D2d	Johnson - Gyrobifastigium (J26)
JETBPY-8	8 D3h	Johnson - Elongated triangular bipyramid (J14)
JBTP-8	9 C2v	Johnson - Biaugmented trigonal prism (J50)
BTPR-8	10 C2v	Biaugmented trigonal prism
JSD-8	11 D2d	Snub disphenoid (J84)
TT-8	12 Td	Triakis tetrahedron
ETBPY-8	13 D3h	Elongated trigonal bipyramid

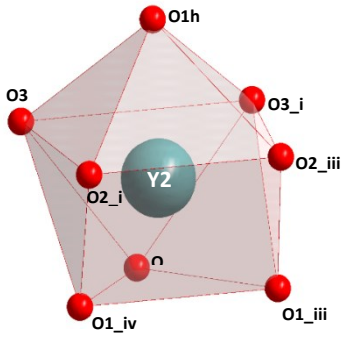

Complex	SAPR-8	TDD-8	JBTPR-8	BTPR-8	JSD-8
Y2	2.927	**2.713**	3.638	3.183	5.487

8. Thermal analysis

Thermogravimetric analyses have been performed over polycrystalline sample in compounds **1** in order to check the stability of the product. The TG curves show two main steps of weight loses. The first steps concerns to the release of the water lattice molecules which are released from room temperature up to 275 ºC. Then, it starts the loss of coordinated DMF molecules, which is somewhat overlapped with the third step corresponding to the decomposition of the ligands. The latter involves the collapse of the crystal structure, evolving to Y_2O_3 that is obtained at 800 ºC as the final residue.

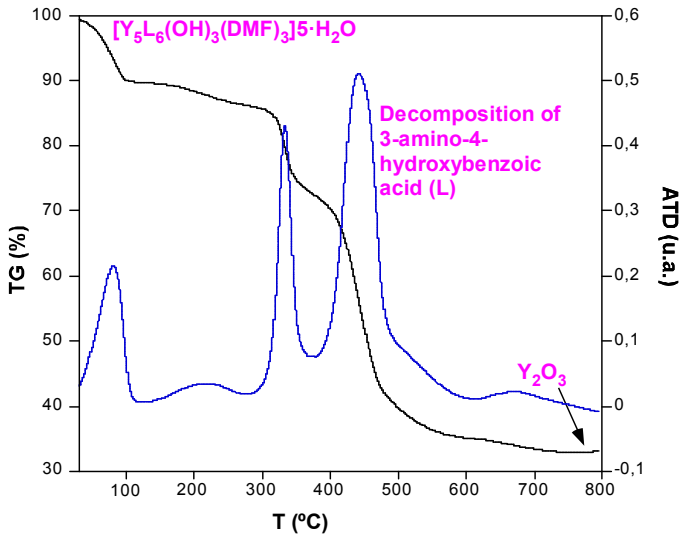

Figure S3. Figure of TG/DTA analysis of compound **1.**

9. Additional views of the structure

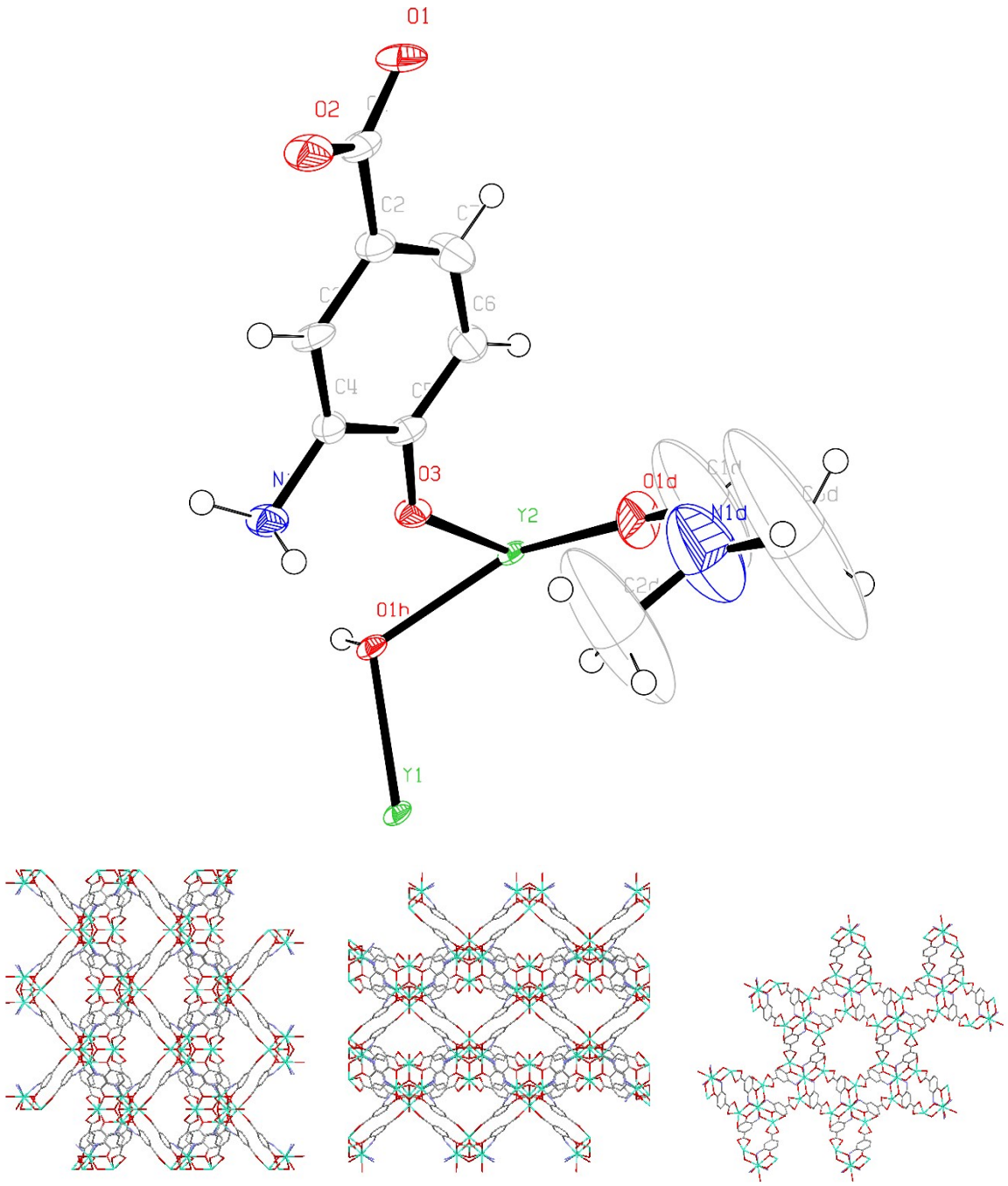

Figure S4. View of the asymmetric unit of complex **1** showing the atomic ADPs (top). Views along a (left), b (middle) and c (right) axis of complex **1** (down). Yttrium, oxygen, nitrogen, and carbon are represented in green, red, blue, and grey, respectively; hydrogen atoms are omitted for clarity.

10. Luminescence properties

The emission spectrum of compound **1** and ligand are sown in Fig. S5. Compound **1** exhibits a broad band where two maxima can be observed at around 385 and 393 nm when it is excited at the wavelength of 325 nm.

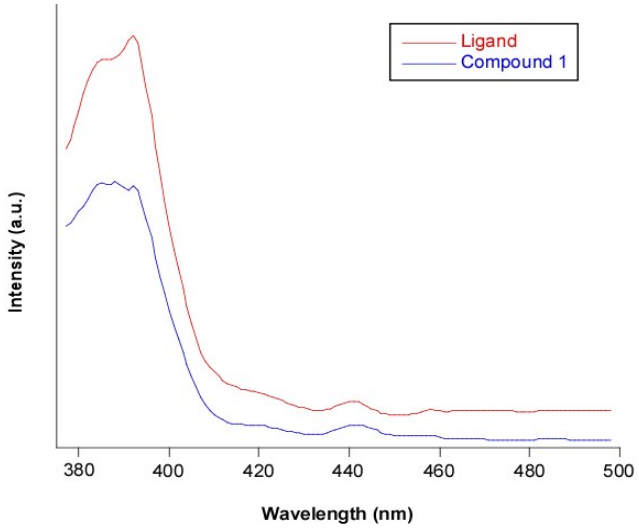

Figure S5. Figure caption of the experimental room temperature photoluminescence emission spectra under λ_{ex} = 325 nm of compounds **1** (blue) and ligand (red).

The excitation spectra have been measured for compound **1** by monitoring the emission maxima. As observed in Figure S6, the excitation spectra show a band covering the 300–350 nm range in which three peaks (sited at *ca*. 307, 322 and 332 nm) are distinguished.

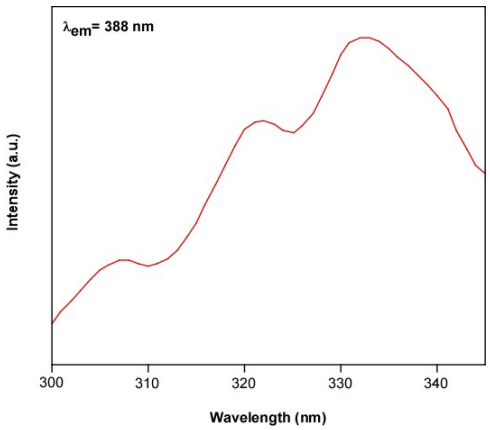

Figure S6. Figure of the excitation spectrum spectra of compound **1** monitored at the emission maxima λ_{em} = 388 nm.

11. Optimization of the reaction conditions

Table S5. Optimization of the reaction conditions.[a]

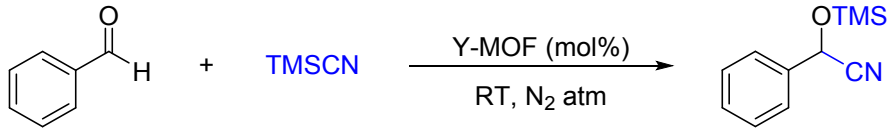

2a **3a**

Entry	Y-MOF (mol%)	time (h)	Ratio (1a:2)	Conv. (%)[b]
1	-	14	1:2	4
2	0.5	14	1:2	>99
3	-	14	1:1.1	8
4	0.5	14	1:1.1	>99
5	0.5	1	1:1.1	53
		3.5		90
		5		>99
6[c]	0.5	5	1:1.1	>99 (86)
7[c]	0.1	5	1:1.1	28
		24		>99 (95)

[a] Reaction carried out using substrates **2a** (25 µL, 0.25 mmol) and TMSCN (34 µL, 0.275 mmol, 1.1 equiv.) under inert N_2 atmosphere at room temperature. [b] Conversions (relative to aldehyde **2a**) determined by ^{1}H NMR of the reaction crude. Isolated yields are given in brackets. [c] Multigram scale reaction carried out with 507 µL (5 mmol) of substrate **2a** and 688 µL (5.5 mmol, 1.1 equiv.) of TMSCN.

12. Characterization Data of Products

2-Phenyl-2-((trimethylsilyl)oxy)acetonitrile (3a). This product has been previously reported.[7] ^{1}H NMR (300.13 MHz, $CDCl_3$): δ 7.50–7.35 (m, 5H, ArH), 5.50 (s, 1H, *CH*CN), 0.23 (s, 9H, TMS) ppm. ^{13}C NMR (75.48 MHz, $CDCl_3$): δ 136.2 (C_{ipso}), 129.3(ArCH), 128.9 (ArCH), 126.3 (ArCH), 119.1 (CN), 63.6 (CH), -0.29 (TMS) ppm.

2-(*p*-Tolyl)-2-((trimethylsilyl)oxy)acetonitrile (3b). This product has been previously reported.[8] ^{1}H NMR (300.13 MHz, $CDCl_3$): δ 7.37 (d, J = 7.9 Hz, 2H, ArH), 7.22 (d, J = 7.9 Hz, 2H, ArH), 5.47 (s, 1H, *CH*CN), 2.38 (s, 3H, CH_3), 0.23 (s, 9H, TMS) ppm. ^{13}C NMR (75.48 MHz, $CDCl_3$): δ 139.3 (C_{ipso}), 133.3 (C_{ispo}), 129.5 (ArCH), 126.3 (ArCH), 119.2 (CN), 63.5 (CH), 21.1 (CH_3), -0.29 (TMS) ppm.

2-(4-Methoxyphenyl)-2-((trimethylsilyl)oxy)acetonitrile (3c). This product has been previously reported.[9] ^{1}H NMR (300.13 MHz, $CDCl_3$): δ 7.38 (d, J = 8.6 Hz, 2H, ArH), 6.92 (d, J = 8.6 Hz, 2H, ArH), 5.43 (s, 1H, *CH*CN), 3.82 (s, 3H, OMe), -0.21 (s, 9H, TMS) ppm. ^{13}C NMR (75.48 MHz, $CDCl_3$): δ 160.3 (C_{ipso}), 128.3 (C_{ipso}), 127.9 (ArCH), 119.3 (CN), 114.2 (ArCH), 63.3 (CH), 55.3 (OCH_3), -0.24 (TMS) ppm.

2-(4-(Dimethylamino)phenyl)-2-((trimethylsilyl)oxy)acetonitrile (3d). ^{1}H NMR (300.13 MHz, $CDCl_3$): δ 7.31 (d, J = 8.7 Hz, 2H, ArH), 6.71 (d, J = 8.7 Hz, 2H, ArH), 5.39 (s, 1H, *CH*CN), 2.98 (s, 6H, NMe_2), 0.19 (s, 9H, TMS) ppm. ^{13}C NMR (75.48 MHz, $CDCl_3$): δ 151.1 (C_{ipso}), 127.8 (ArCH), 123.6 (C_{ipso}), 119.6 (CN), 112.1 (ArCH), 63.7 (CH), 40.3 (CH_3), -0.16 (TMS) ppm. IR (ATR): ν 2959 (CH_3), 2230 (C≡N), 1621 (C=N), 1531 (C=C), 1371 (C-N), 1257 (C-O), 1061 (C-O), 835 cm^{-1}. Elemental Analysis calc. for $C_{13}H_{20}N_2OSi$: C 62.86, N, 11.28, H 8.12; found: C 63.23, N 11.65, H 7.67.

2-(3-Fluorophenyl)-2-((trimethylsilyl)oxy)acetonitrile (3e). This product has been previously reported.[10] ^{1}H NMR (300.13 MHz, $CDCl_3$): δ 7.45–7.35 (m, 1H, ArH), 7.25–7.15 (m, 2H, ArH), 7.10–7.05 (m, 1H, ArH), 5.50 (s, 1H, *CH*CN), 0.25 (s, 9H, TMS) ppm. ^{13}C NMR (75.48 MHz, $CDCl_3$): δ 162.8 (d, C_{ipso}, $^{1}J_{C\text{-}F}$ = 247.7 Hz,), 138.6 (d, C_{ipso}, $^{3}J_{C\text{-}F}$ = 7.8 Hz,), 130.5 (d, ArCH, $^{3}J_{C\text{-}F}$ = 8.1 Hz,), 121.7 (d, ArCH, $^{4}J_{C\text{-}F}$ = 3.0 Hz,), 118.7 (CN), 116.3 (d, ArCH, $^{2}J_{C\text{-}F}$ = 21.2 Hz,), 113.3 (d, ArCH, $^{2}J_{C\text{-}F}$ = 23.4 Hz,), 62.8 (d, CH, $^{4}J_{C\text{-}F}$ = 2.1 Hz,), -0.4 (TMS) ppm. ^{19}F-NMR (282.4 MHz, $CDCl_3$): δ -111.4 ppm.

2-(4-Chlorophenyl)-2-((trimethylsilyl)oxy)acetonitrile (3f). This product has been previously reported.[11] ^{1}H NMR (300.13 MHz, $CDCl_3$): δ 7.45–7.40 (m, 5H, ArH), 5.49 (s, 1H, *CH*CN), 0.26 (s, 9H, TMS) ppm. ^{13}C NMR (75.48 MHz, $CDCl_3$): δ 135.3 (C_{ipso}), 134.8 (C_{ipso}), 129.1 (ArCH), 127.7 (ArCH), 118.8 (CN), 63.0 (CH), -0.30 (TMS) ppm.

2-(4-Nitrophenyl)-2-((trimethylsilyl)oxy)acetonitrile (3g). This product has been previously reported.[11] ^{1}H NMR (300.13 MHz, $CDCl_3$): δ 8.29 (d, J = 8.8 Hz, 2H, ArH), 7.67 (d, J = 8.8 Hz, 2H, ArH), 5.59 (s, 1H, *CH*CN), 0.29 (s, 9H, TMS) ppm. ^{13}C NMR (75.48 MHz, $CDCl_3$): δ 148.4 (C_{ipso}), 142.8 (C_{ispo}), 127.0 (ArCH), 124.1 (ArCH), 118.1 (CN), 62.6 (CH), -0.40 (TMS) ppm.

2-(Pyridin-2-yl)-2-((trimethylsilyl)oxy)acetonitrile (3h). This product has been previously reported.[12] ^{1}H NMR (300.13 MHz, $CDCl_3$): δ 8.60–8.55 (m, 1H, ArH), 7.79 (dt, *J* = 7.7, 1.7 Hz, 1H, ArH), 7.59 (d, *J* = 7.7 Hz, 1H, ArH), 7.35–7.25 (m, 1H, ArH), 5.58 (s, 1H, *CH*CN), 0.26 (s, 9H, TMS) ppm. ^{13}C NMR (75.48 MHz, $CDCl_3$): δ 155.4 (C_{ipso}), 149.3 (ArCH), 137.5(ArCH), 124.0 (ArCH), 120.5 (ArCH), 118.6 (CN), 65.1 (CH), -0.37 (TMS) ppm.

2-(Quinolin-2-yl)-2-((trimethylsilyl)oxy)acetonitrile (3i). ^{1}H NMR (300.13 MHz, $CDCl_3$): δ 8.27 (d, *J* = 8.5 Hz, 1H, ArH), 8.09 (d, *J* = 8.5 Hz, 1H, ArH), 7.85 (d, *J* = 8.1 Hz, 1H, ArH), 7.80–7.70 (m, 2H, ArH), 7.60–7.55 (m, 1H, ArH), 5.75 (s, 1H, *CH*CN), 0.27 (s, TMS) ppm. ^{13}C NMR (75.48 MHz, $CDCl_3$): δ 155.4 (C_{ipso}), 147.2 (C_{ipso}), 137.9 (ArCH), 130.1 (ArCH), 129.3 (ArCH), 128.0 (C_{ipso}), 127.6 (ArCH), 127.3 (ArCH), 118.6 (CN), 117.8 (ArCH), 65.9 (CH), -0.31 (TMS) ppm. IR (ATR): ν 3058 (Csp^2-H), 2959 (CH_3), 2170 (C≡N), 1593 (C=N), 1504 (C=C), 1254 (C-O), 1046 (C-O), 838, 774 cm^{-1}. Elemental Analysis calc. for $C_{14}H_{16}N_2OSi$: C 65.59, N, 10.93, H 6.29; found: C 64.85, N 10.66, H 5.98.

2-(Furan-2-yl)-2-((trimethylsilyl)oxy)acetonitrile (3j). This product has been previously reported.[13] ^{1}H NMR (300.13 MHz, $CDCl_3$): δ 7.45 (d, *J* = 1.7 Hz, 1H, CH), 6.54 (d, *J* = 3.3 Hz, 1H, CH), 6.40 (dd, *J* = 3.3, 1.7 Hz, 1H, CH), 5.54 (s, 1H, *CH*CN), 0.19 (s, 9H, TMS) ppm. ^{13}CNMR (75.48 MHz, $CDCl_3$): δ 148.2 (C), 143.8 (FurCH), 117.1 (CN), 110.8 (FurCH), 109.7 (FurCH), 57.4 (CH), -0.42 (TMS) ppm.

2-(Thiophen-2-yl)-2-((trimethylsilyl)oxy)acetonitrile (3k). This product has been previously reported.[14] ^{1}H NMR (300.13 MHz, $CDCl_3$): δ 7.37 (d, *J* = 5.3 Hz, 1H, CH), 7.20–7.15 (m, 1H, CH), 7.05–7.00 (m, 1H, CH), 5.73 (s, 1H, *CH*CN), 0.23 (s, 9H, TMS) ppm. ^{13}C NMR (75.48 MHz, $CDCl_3$): δ 139.5 (C), 127.2 (TiophCH), 126.9 (TiophCH), 126.3 (TiophCH), 118.3 (CN), 59.5 (CH), -0.31 (TMS) ppm.

2-((Trimethylsilyl)oxy)butanenitrile (3l). This product has been previously reported.[15] ^{1}H NMR (300.13 MHz, $CDCl_3$): δ 4.34 (t, J = 6.3 Hz, 1H, CH), 1.85–1.75 (m, 2H, CH_2), 1.04 (t, J = 7.4 Hz, 3H, CH_3), 0.21 (s, 9H, CH_3 x 3) ppm. ^{13}C NMR (75.48 MHz, $CDCl_3$): δ 119.9 (CN), 62.7 (CH), 29.6 (CH_2), 8.9 (CH_3), 0.4 (TMS) ppm.

(*E*)-4-Phenyl-2-((trimethylsilyl)oxy)but-3-enenitrile (3m). This product has been previously reported.[16] ^{1}H NMR (300.13 MHz, $CDCl_3$): δ 7.45–7.30 (m, 5H, ArH), 6.82 (d, *J* = 15.8 Hz, 1H, CH), 6.20 (dd, *J* = 15.8, 6.0 Hz, 1H, CH), 5.13 (d, *J* = 6.0 Hz, 1H, CH), 0.26 (s, 9H, TMS) ppm. ^{13}C NMR (75.48 MHz, $CDCl_3$): δ 135.0 (C_{ipso}). 133.9 (CH), 128.76 (ArCH), 128.71 (ArCH), 126.96 (ArCH), 123.5 (CH), 118.4 (CN), 62.2 (CH), 0.15 (TMS) ppm.

2-Phenyl-2-((trimethylsilyl)oxy)propanenitrile (3n). This product has been previously reported.[17] ^{1}H NMR (300.13 MHz, $CDCl_3$): δ 7.60–7.50 (m, 2H, ArH), 7.45–7.30 (m, 3H, ArH), 1.86 (s, 3H, CH_3), 0.18 (s, 9H, TMS) ppm. ^{13}C NMR (75.48 MHz, $CDCl_3$): δ 142.0

(C_{ipso}), 128.68 (ArCH), 128.66 (ArCH), 124.6 (ArCH), 121.6 (CN), 71.6 (C), 33.5 (CH_3), 1.03 (TMS) ppm.

2-(4-Isobutylphenyl)-2-((trimethylsilyl)oxy)propanenitrile (3o). This product has been previously reported.[18] ^{1}H NMR (300.13 MHz, $CDCl_3$): δ 7.44 (d, *J* = 8.2 Hz, 2H, ArH), 7.16 (d, *J* = 8.2 Hz, 2H, ArH), 2.49 (d, *J* = 7.2 Hz, 2H, CH_2), 1.90–1.80 (m, 4H, CH, CH_3), 0.90 (d, *J* = 6.6 Hz, 6H, 2 x CH_3), 0.16 (s, 9H, TMS) ppm. ^{13}C NMR (75.48 MHz, $CDCl_3$): δ 142.3 (C_{ipso}), 139.2 (C_{ipso}), 129.3 (ArCH), 124.5 (ArCH), 121.8 (CN), 71.5 (C), 44.9 (CH_2), 33.4 (CH_3), 30.1 (CH_3), 22.3 (CH_3), 1.04 (TMS) ppm.

2,2-Diphenyl-2-((trimethylsilyl)oxy)acetonitrile (3p). This product has been previously reported.[19] ^{1}H NMR (300.13 MHz, $CDCl_3$): δ 7.55–7.50 (m, 4H, ArH), 7.40–7.35 (m, 6H, ArH), 0.15 (s, 9H, TMS) ppm. ^{13}C NMR (75.48 MHz, $CDCl_3$): δ 141.9 (C_{ipso}), 128.6 (ArCH), 128.5 (ArCH), 125.9 (ArCH), 120.7 (CN), 76.3 (C), 0.9 (TMS) ppm.

2-Methyl-2-((trimethylsilyl)oxy)butanenitrile (3q). This product has been previously reported.[20] ^{1}H NMR (300.13 MHz, $CDCl_3$): δ 1.85–1.65 (m, 2H, CH_2), 1.55 (s, 3H, CH_3), 1.04 (t, *J* = 7.4 Hz, 3H, CH_3CH_2), 0.23 (s, 9H, TMS) ppm. ^{13}C NMR (75.48 MHz, $CDCl_3$): δ 121.9 (CN), 70.2 (C), 36.4 (CH_2), 28.4 (CH_3), 8.6 (CH_3), 1.21 (TMS) ppm.

1-((Trimethylsilyl)oxy)cyclohexane-1-carbonitrile (3r). This product has been previously reported.[21] ^{1}H NMR (300.13 MHz, $CDCl_3$): δ 2.10–2.00 (m, 2H, CH_2), 1.75–1.70 (m, 2H, CH_2), 1.70–1.45 (m, 6H, CH_2 x 3), 1.30–1.20 (m, 2H, CH_2), 0.23 (s, 9H, TMS) ppm. ^{13}C NMR (75.48 MHz, $CDCl_3$): δ 121.9 (CN), 70.6 (C), 39.3 (CH_2), 24.5 (CH_2), 22.6 (CH_2), 1.38 (TMS) ppm.

1-((Trimethylsilyl)oxy)-1,2,3,4-tetrahydronaphthalene-1-carbonitrile (3s). This product has been previously reported.[22] ^{1}H NMR (300.13 MHz, $CDCl_3$): δ 7.70–7.60 (m, 1H, ArH), 7.30–7.20 (m, 2H, ArH), 7.15–7.05 (m, 1H, ArH), 2.85–2.80 (m, 2H), 2.40–2.30 (m, 1H), 2.25–2.15 (m, 1H), 2.10–1.95 (m, 2H), 0.21 (s, 9H, TMS) ppm. ^{13}C NMR (75.48 MHz, $CDCl_3$): δ 136.1 (C_{ipso}), 135.7 (C_{ipso}), 129.3 (ArCH), 129.1 (ArCH), 128.0 (ArCH), 126.6 (ArCH), 122.1 (CN), 69.6 (C), 37.7 (CH_2), 28.3 (CH_2), 18.7 (CH_2), 1.3 (TMS) ppm.

2-((Trimethylsilyl)oxy)adamantane-2-carbonitrile (3t). This product has been previously reported.[23,24] ^{1}H NMR (300.13 MHz, $CDCl_3$): δ 2.20–2.00 (m, 6H), 1.95–1.80 (m, 3H), 1.80–1.65 (m, 3H), 1.60–1.50 (m, 2H), 0.25 (s, 9H, TMS) ppm. ^{13}C NMR (75.48 MHz, $CDCl_3$): δ 122.1 (CN), 74.7 (C), 38.1 (CH), 37.2 (CH_2), 34.7 (CH_2), 30.9 (CH_2), 26.3 (CH), 26.1 (CH), 1.2 (TMS) ppm.

2,2-Dicyclohexyl-2-((trimethylsilyl)oxy)acetonitrile (3u). ^{1}H NMR (300.13 MHz, $CDCl_3$): δ 1.90–1.75 (m, 8H), 1.70–1.60 (m, 4H), 1.30–1.05 (m, 10H, CH_2), 0.23 (s, 9H, TMS) ppm. ^{13}C NMR (75.48 MHz, $CDCl_3$): δ 120.5 (CN), 80.6 (C), 43.6 (CH), 28.3 (CH_2), 26.4 (CH_2), 26.2 (CH_2), 26.1 (CH_2), 1.9 (TMS) ppm. IR (ATR): ν 2931 (CH_2),

2858 (CH_2), 1451, 1249, 1123, 1023, 842, 766 cm^{-1}. Elemental Analysis calc. for $C_{17}H_{31}NOSi$: C 69.56, N 4.77, H 10.65; found: C 69.62, N 4.68, H 10.21.

13.NMR Spectra of New Compounds

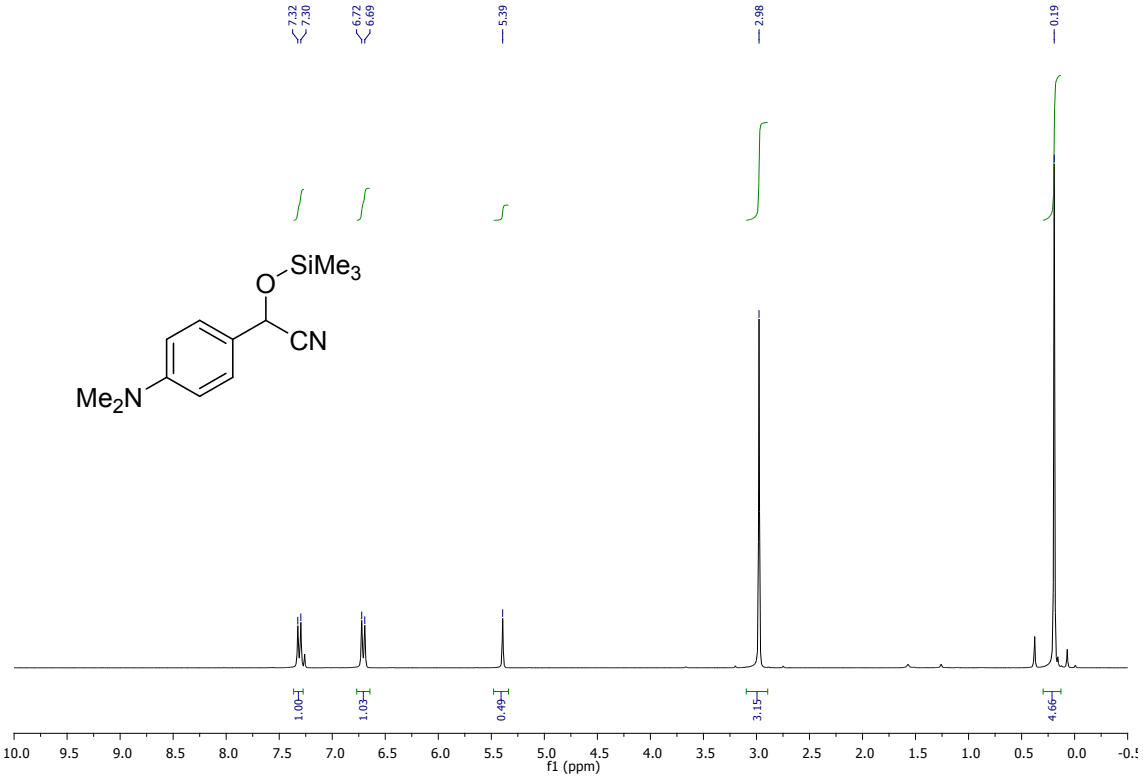

Figure S7. ^{1}H NMR (300.13 MHz, $CDCl_3$) spectrum of **3d**.

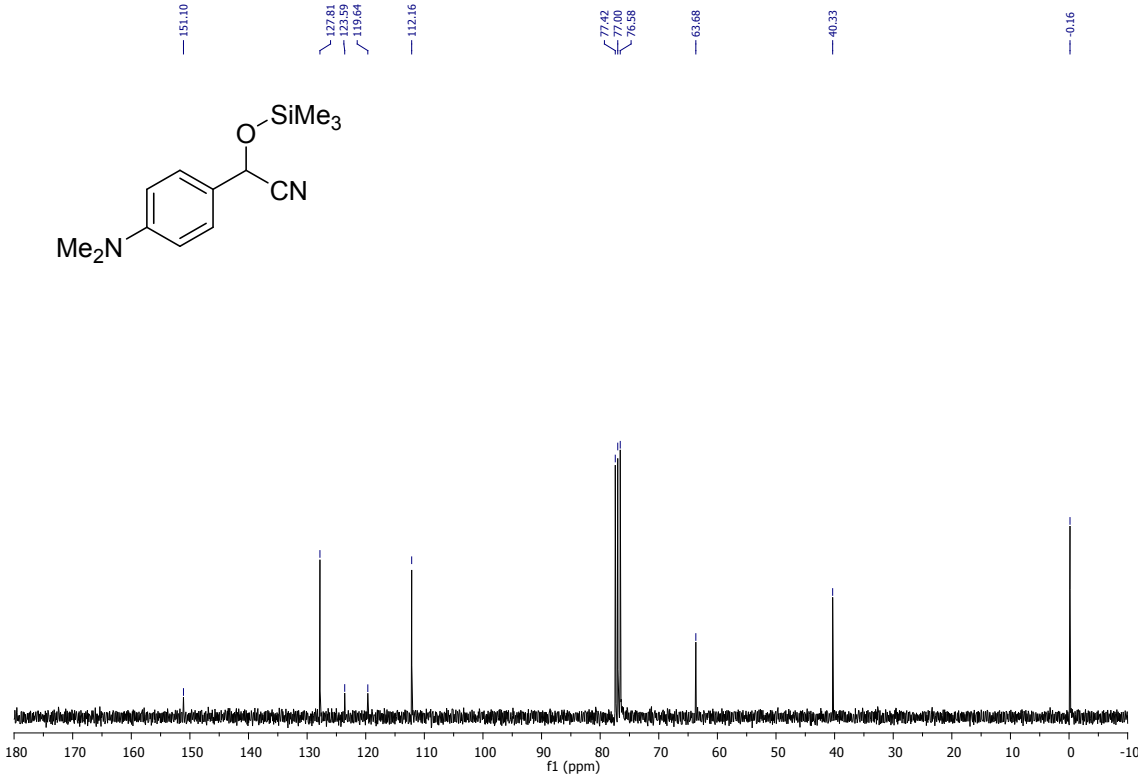

Figure S8. ^{13}C NMR (75.48 MHz, $CDCl_3$) spectrum of **3d**.

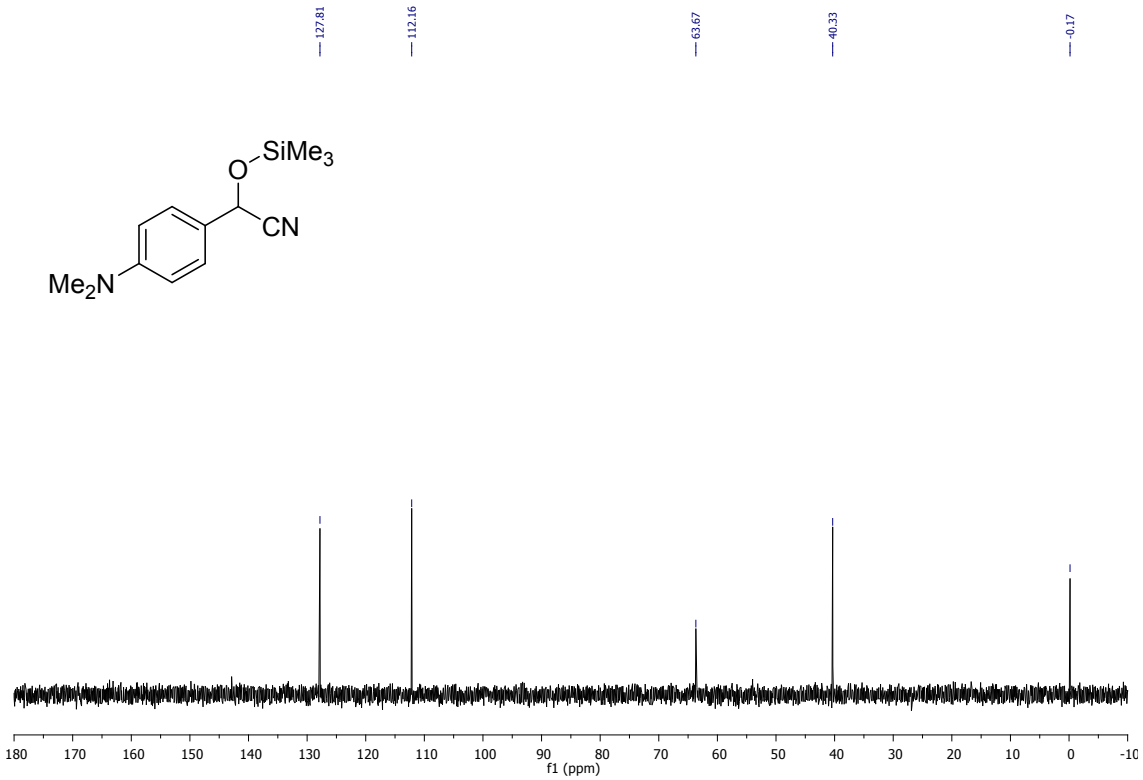

Figure S9. DEPT-135 spectrum of **3d**.

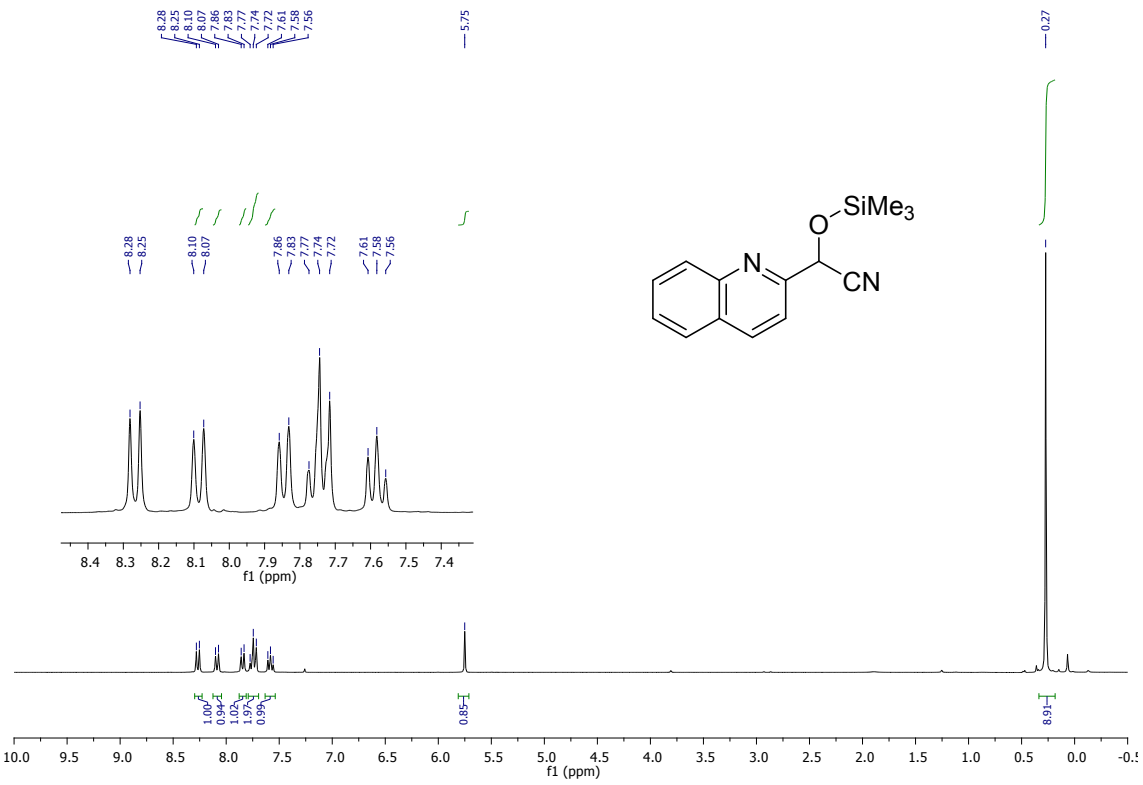

Figure S10. ^{1}H NMR (300.13 MHz, $CDCl_3$) spectrum of **3i**.

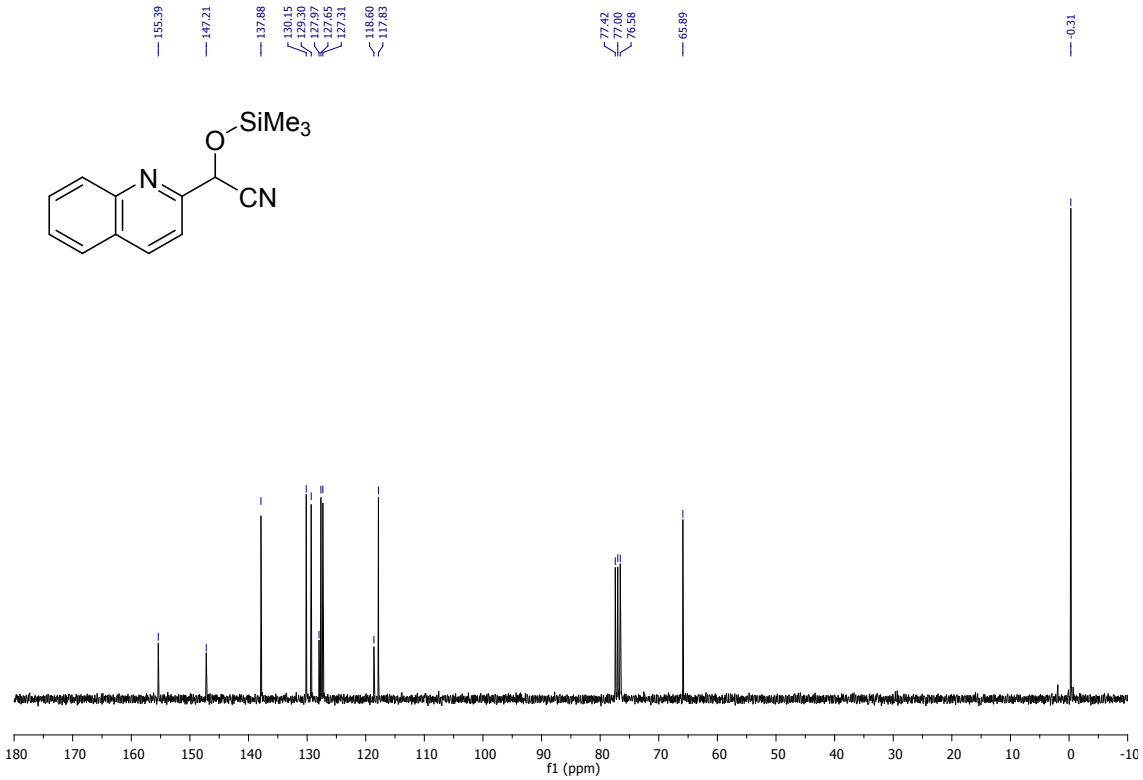

Figure S11. ^{13}C NMR (75.48 MHz, $CDCl_3$) spectrum of **3i**.

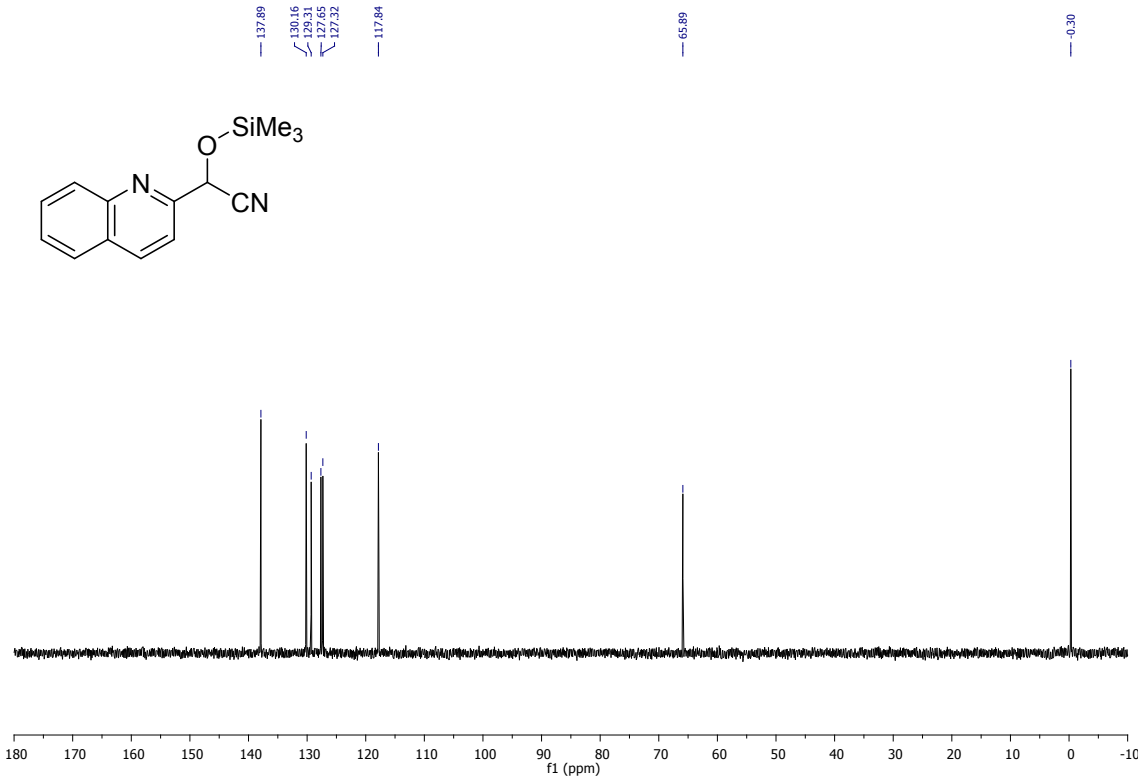

Figure S12. DEPT-135 spectrum of **3i**.

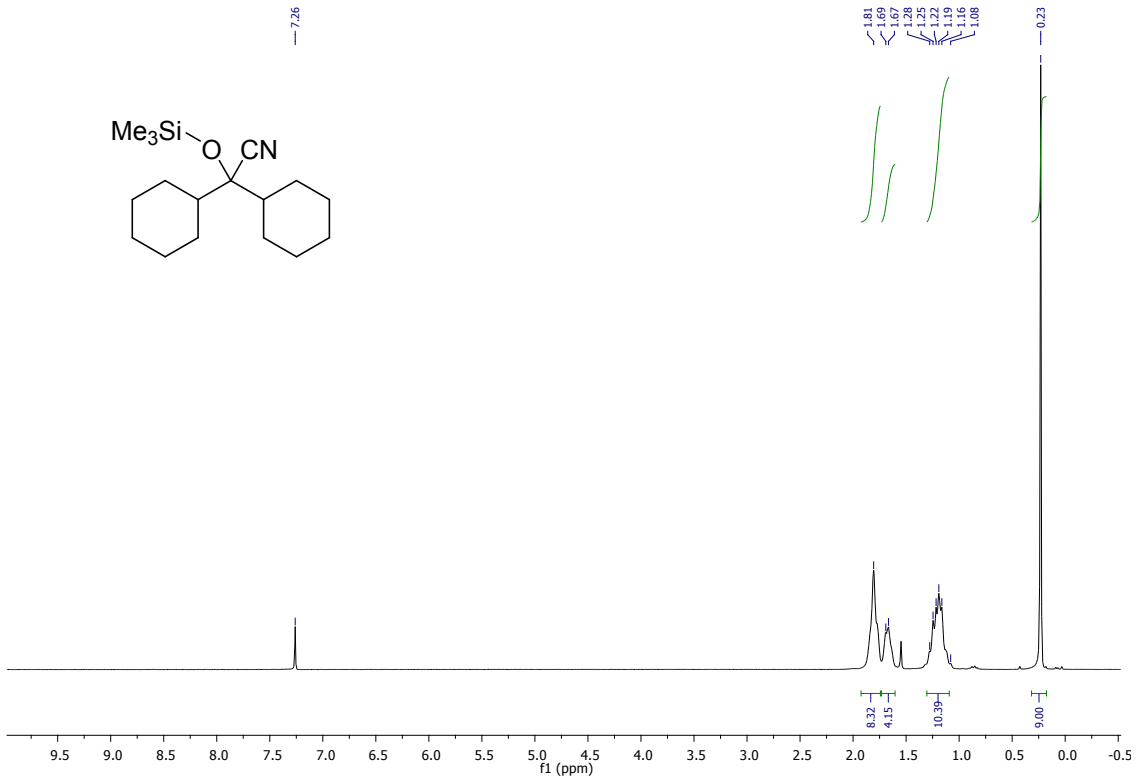

Figure S13. ^{1}H NMR (300.13 MHz, $CDCl_3$) spectrum of **3u**.

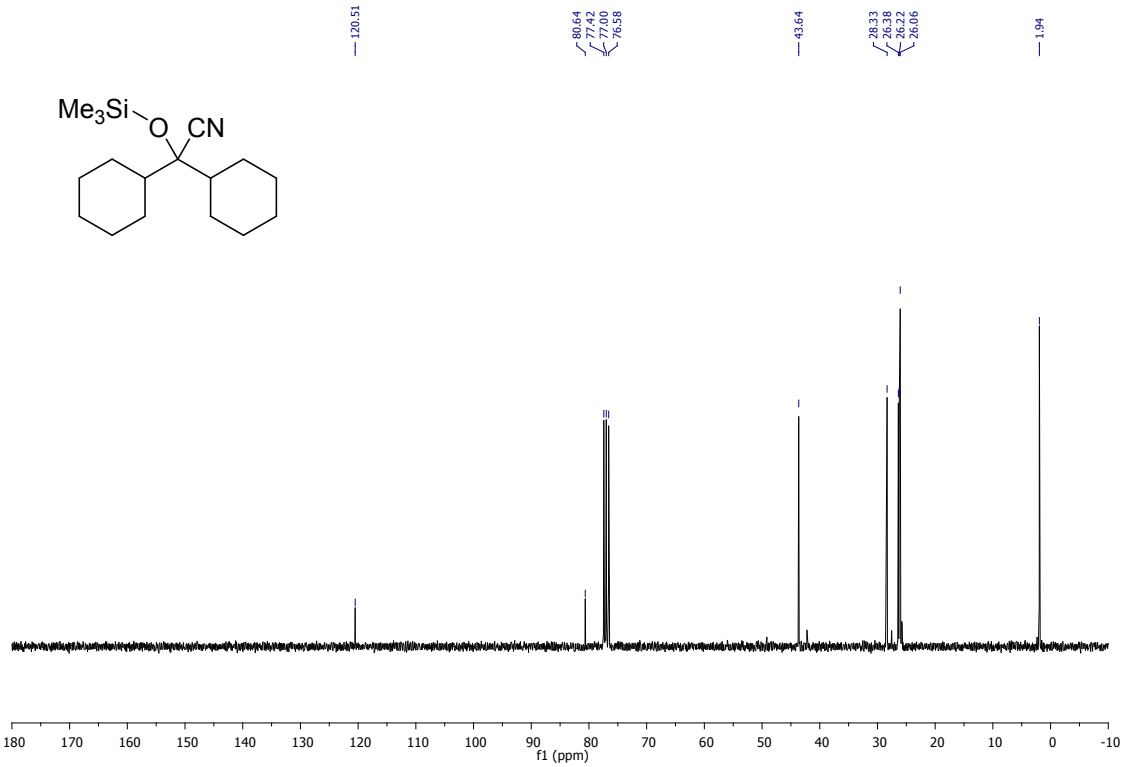

Figure S14. ^{13}C NMR (75.48 MHz, $CDCl_3$) spectrum of **3u**.

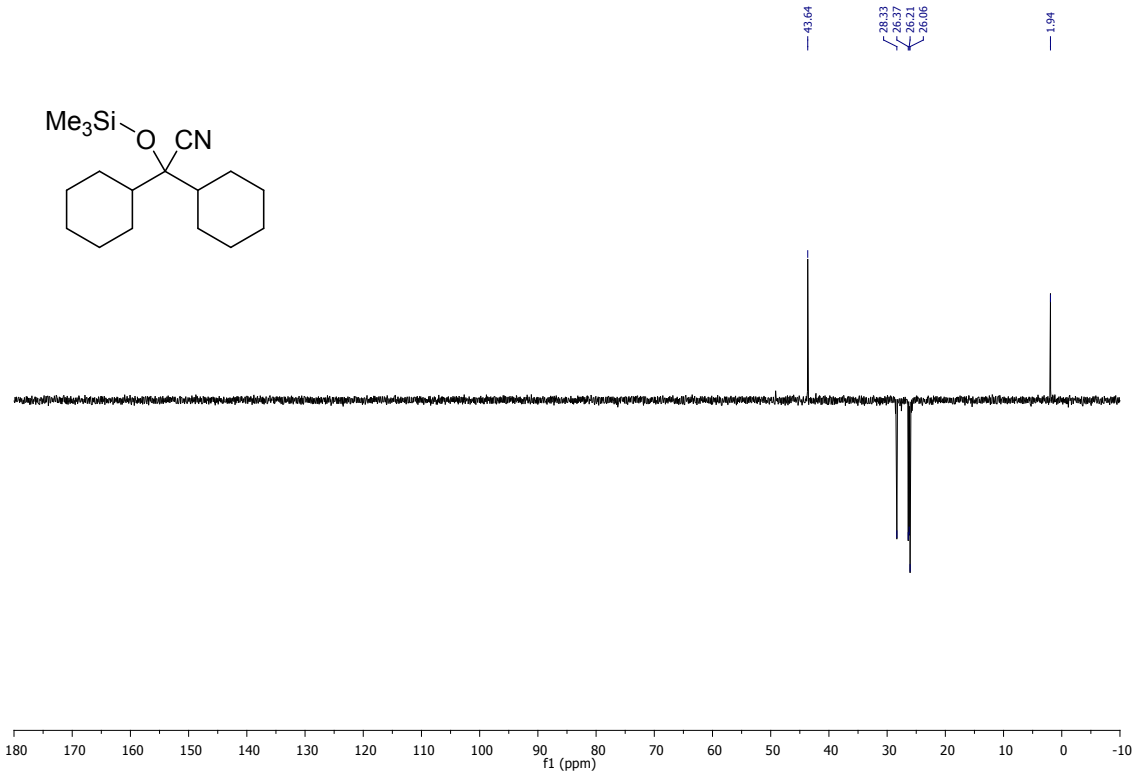

Figure S15. DEPT-135 spectrum of **3u**.

14. IR Spectra of New Compounds

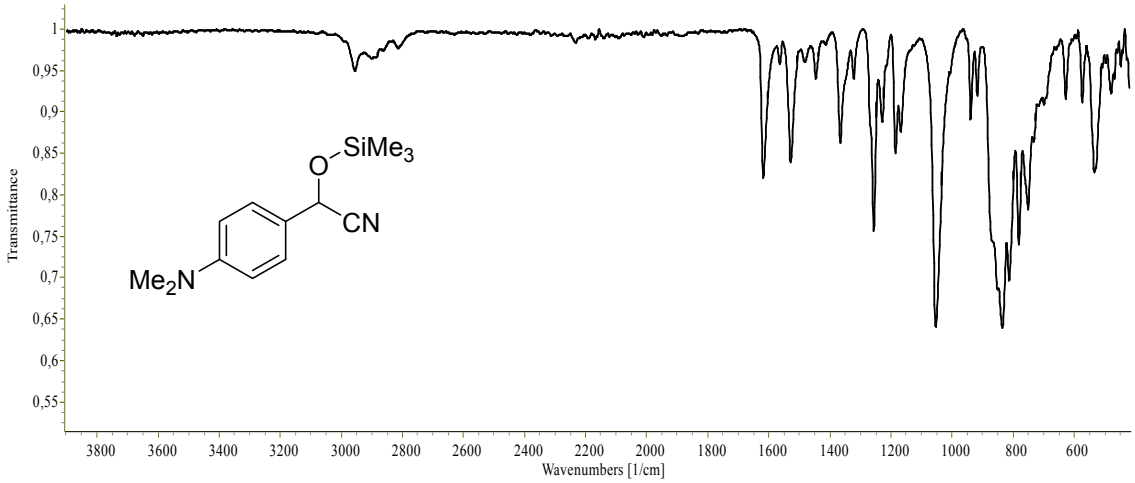

Figure S16. IR (ATR) spectra of compound **3d**.

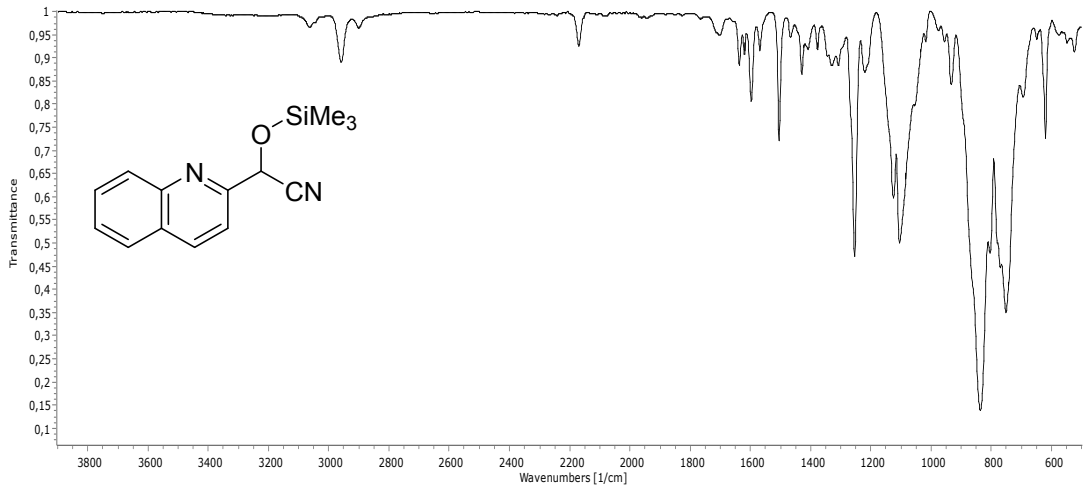

Figure S17. IR (ATR) spectra of compound **3i**.

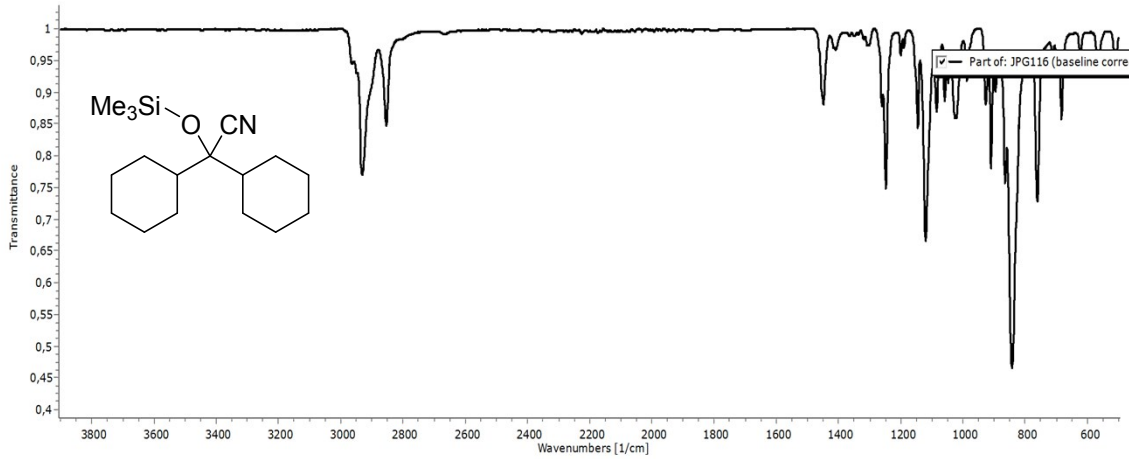

Figure S18. IR (ATR) spectra of compound **3i**.

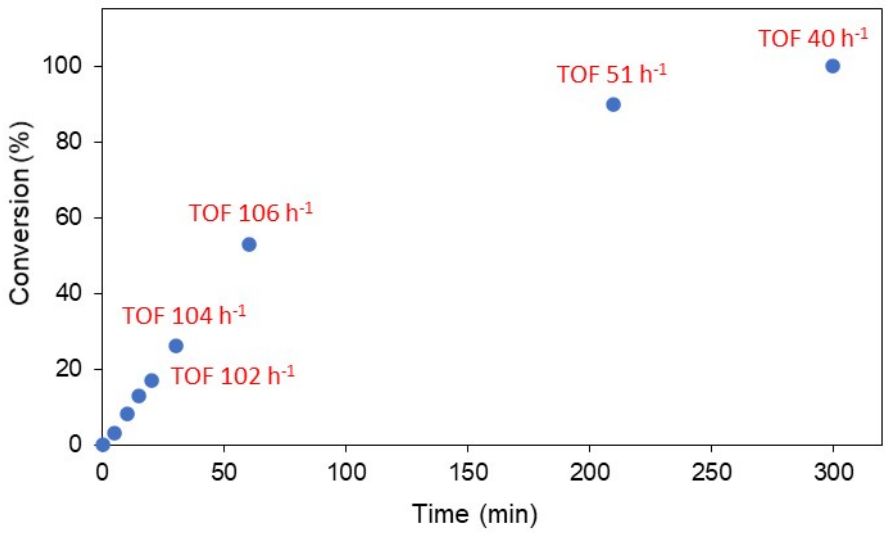

Figure S18. Kinetic profile for the cyanosilylation of benzaldehyde under optimized conditions. Numbers in red are TOF values calculated for some of the achieved conversions.

15. Catalyst Recyclability

Recyclability of the catalyst: In a 1 mL vial with a septum screw capped equipped with a stirring bar, the catalyst Y-MOF (2.3 mg, 0.5 mol%) was weighed. Then, the corresponding amount of carbonylic compound **2a** (25 µL, 0.25 mmol) followed by TMSCN (34 µL, 0.275 mmol, 1.1 equiv.) were added and the reaction was stirred under inert N_2 atmosphere at room temperature during 5 h. After this time, 1.5 mL of DCM was added to the reaction mixture and transferred to a centrifuge tube for the separation of the catalyst. The centrifugation of the mixture was carried out at 8000 rpm during 3 min. After that, the solution was eliminated, and the catalyst was washed with DCM (2 x 1.5 mL). Later on, the catalyst was dried under vacuum and reused in the next cycle of the reaction with the same reaction conditions previously described.

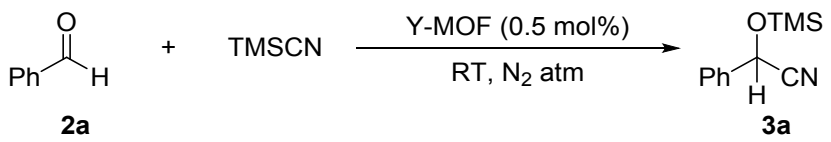

Scheme S1. Reaction conditions used for the study of recyclability of catalyst **1**.

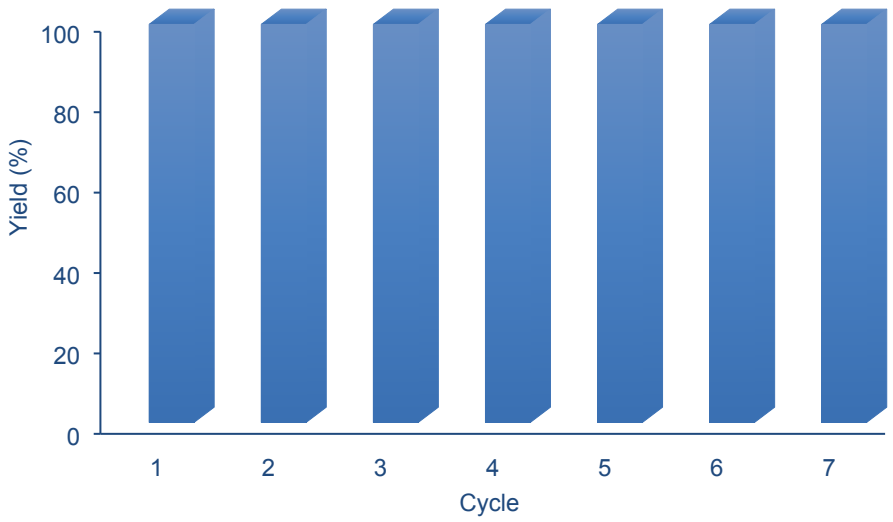

Figure S19. Recyclability of catalyst **1** during 7 consecutive cycles.

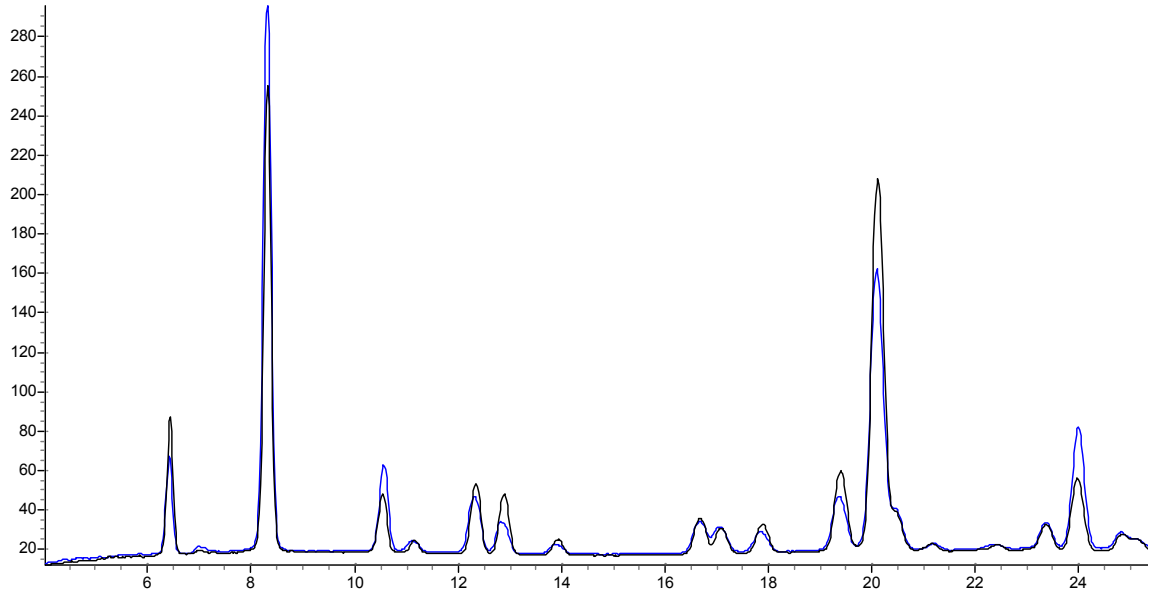

Figure S20. Powder XR patterns showing the recyclability of catalyst **1** before and after the cycles.

16. Leaching test

Leaching test: after the second reaction of the recyclability test was complete, the reaction was centrifuged and the supernatant was dried under vacuum and then compound **2k** (21 µL, 0.25 mmol) and TMSCN (34 µL, 0.275 mmol, 1.1 equiv.) were added and the reaction was stirred under inert N_2 atmosphere at room temperature. An aliquot was analysed by ^{1}H NMR after 5 and 24 hours obtaining only 6% of product **3k**.

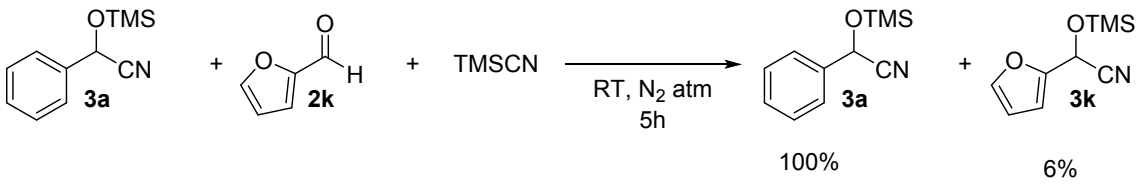

Scheme S2. Leaching test.

17. View of possible active sites in pores

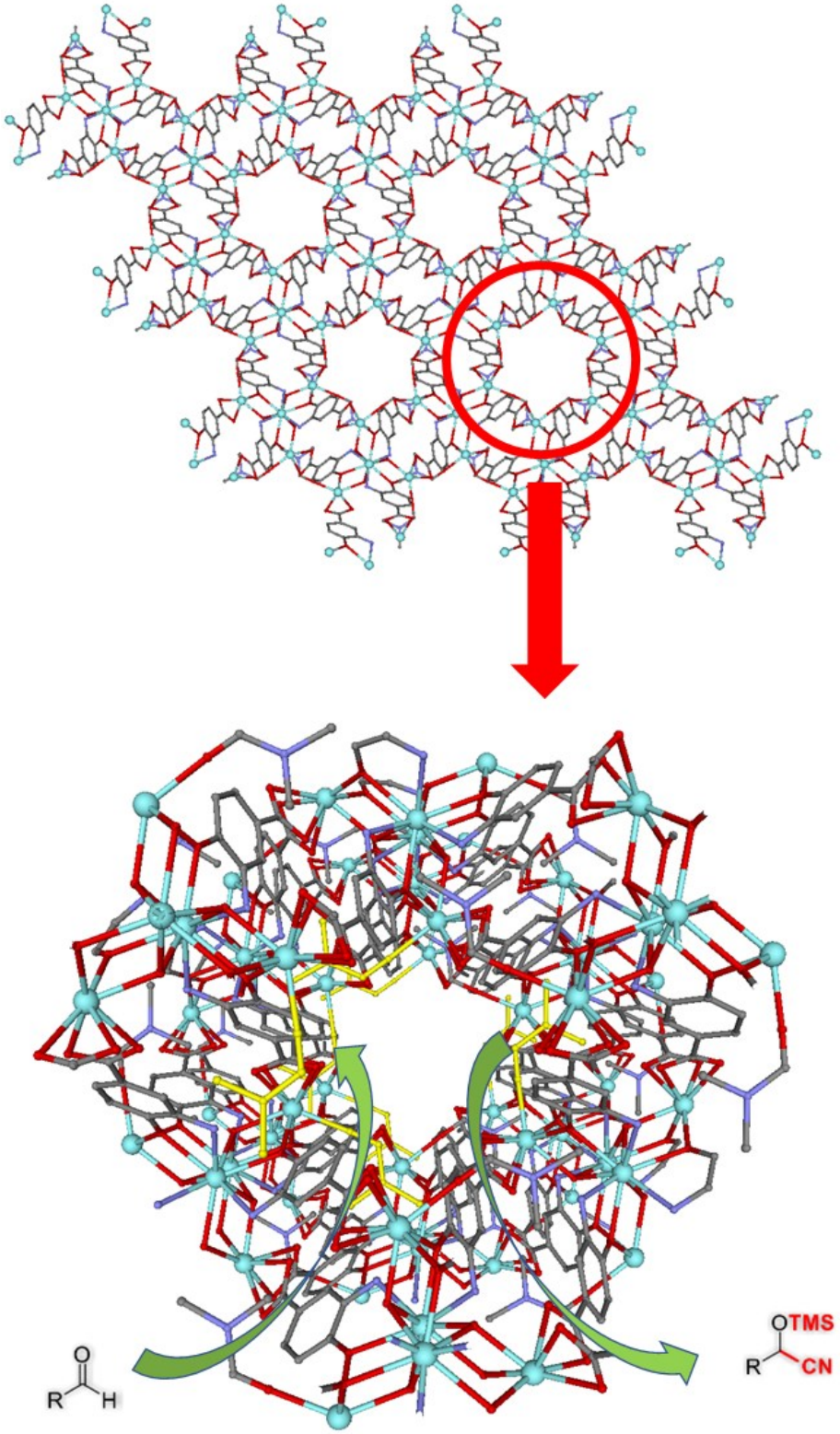

Figure S21. View of proposed possible active sites in pores. Coordinated DMF molecules (marked in yellow) occupy the unsaturated positions of the metal atoms in the pores.

18. Proposed mechanisms for the MOF-catalyzed cyanosilylation reaction

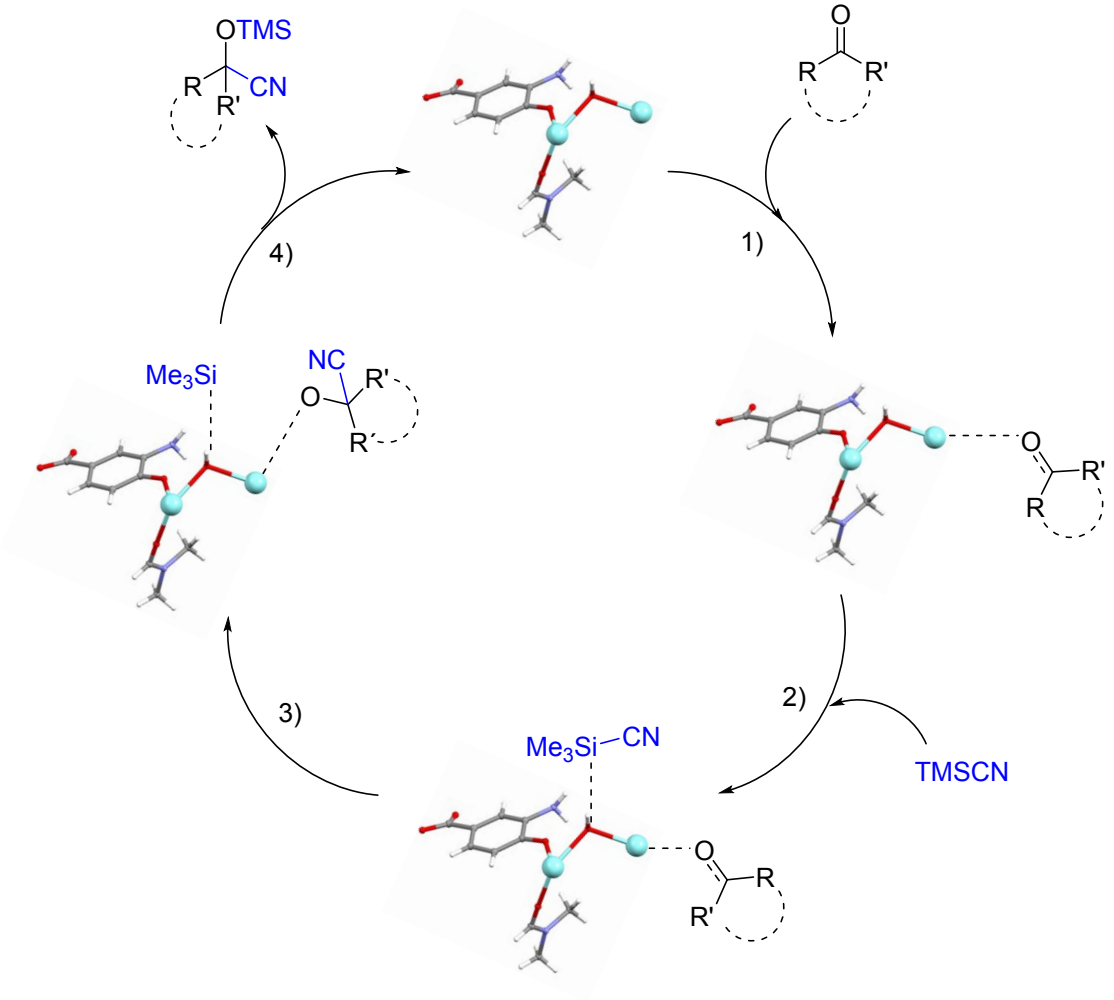

Scheme S3. Proposed mechanism (four steps) for the MOF-catalyzed cyanosilylation reaction.

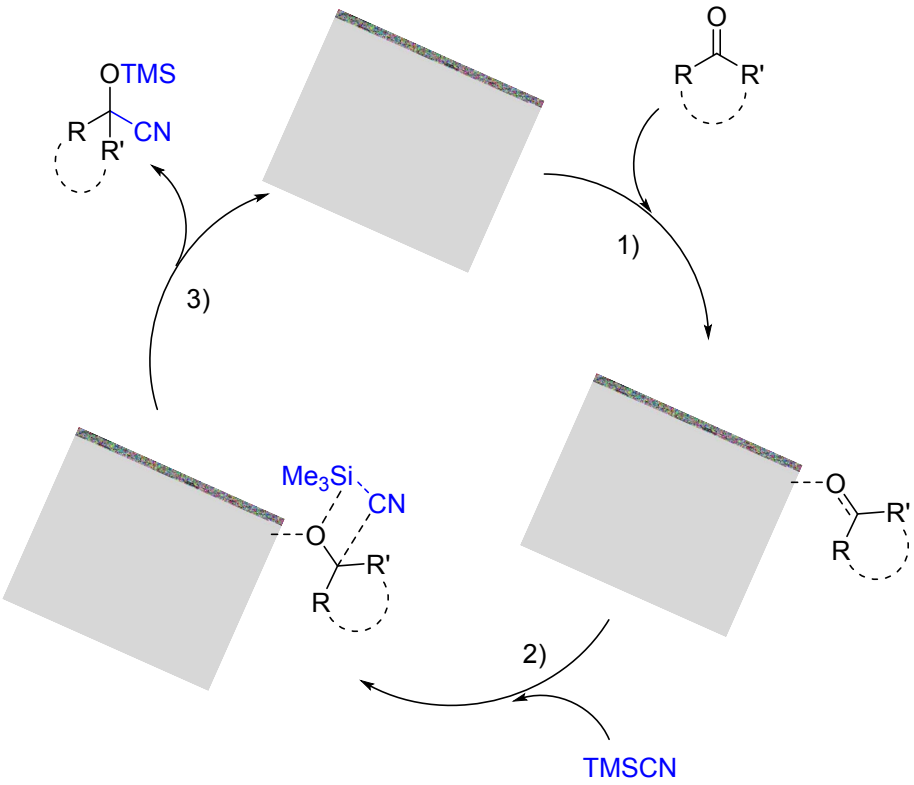

Scheme S4. Proposed mechanism (three steps) for the MOF-catalyzed cyanosilylation reaction.

19. Results obtained with different lanthanides MOF catalysts.

Table S6. Catalytic cyanosilylation of benzaldehyde performances of Ln-MOFs reported in the literature.

MOF	mol%	Recyclability	Conv.	Conditions	Ratio[a]	TOF	Ref.
$Eu_2(MELL)(H_2O)_6$[b]	10	5 cycles	>99% (3h)	RT, MeCN	1:2	3.2 h^{-1}	25
[Sm/Dy/Yb(3,5-DSB)(Phen)(H_2O)]·H_2O[c]	2	4 cycles	>99% (3h) (Sm) 70%, 3h (Dy) 50%, 3h (Yb)	40 °C,	1:1.5	6-79 h^{-1}	26–28
Sm/Eu/Gd/Tb/Eu-Gd/Eu-Tb-psa[d]	5	3 cycles	70%, <2h (Eu) 80%, <2h (Sm) 87%, <2h (Eu-Gd) 74%, <2h (Tb) 94%, <2h (Eu-Tb)	RT, DCM	1:1.5	84-112 h^{-1}	29
Nd/Eu/Sm/Ho/Yb/Er-dms[e]	5	3 cycles	85%, <1h (Nd) 96%, <1h (Eu) 92%, <2h (Sm) 79%, <2h (Ho) 98%, <2h (Yb) 93%, <2h (Er)	RT, DCM	1:1.5	159-234 h^{-1}	30
Nd, Ho, Er, Yb-btc[f]	4.5	5 cycles	>99%, 2h	RT, DCM	1:2	1-11 h^{-1}	31
$Tm(BDC)_{1.5}$(DMF)-(H_2O)[g]	2	[h]	57%, 5h	RT	1:1	[h]	32
La/Ce/Nd/Sm/Dy(L)$(NO_3)(DMF)_2]_n$·n(DMF)[i]	3	5 cycles	93%, 2h (La) 94%, 2h (Ce) 91%, 2h (Nd) 89%, 2h (Sm) 90%, 2h (Dy)	RT	1:4	2-16 h^{-1}	33
Tb-TCA[j]	2	[h]	78%, 4h	RT, DCM[k]	1:2.4	9.8 h^{-1}	34
[Sm(L-H_2)(R-L-H_3)(H_2O)$_4$]·nH_2O[l]	10	[h]	69%, 16h	RT, DCM	1:2	0.4 h^{-1}	35

$[Yb_2(L)_2(H_2O)_3]\cdot 2H_2O$[m]	1.4	5 cycles	>99%, 24h	RT	1:2	5 h^{-1}	[36]
$[Pr(L^{OMe})(H_2O)_4]\cdot 2.5DMA\cdot 3H_2O$[n]	1.9	2 cycles	99%, 14h	RT	1:2	3.8 h^{-1}	[37]
$[Sm(H_2O)_5][Sm(H_2O)_7][Co_2Mo_{10}H_4O_{38}]\cdot 6H_2O$	2	3 cycles	98%, 5h	RT	1:3	9.8 h^{-1}	[38]
$[La/Ce/Nd(H_2O)_5]_2Mo_6V_2O_{26}\cdot 8H_2O$	1	3 cycles	94%, 5h (La) 90%, 5h (Ce) 96%, 5h (Nd)	RT	1:3	10.4 h^{-1} 10.0 h^{-1} 13.7 h^{-1}	[39]
Our Y-MOF catalyst (**1**)	0.5	7 cycles	>99%, 5h	RT	1:1	51 h^{-1}	This work

[a] Ratio between benzaldehyde and TMSCN; [b] MELL = mellitic acid; [c] 3,5-DSB = 3,5-disulfobenzoate, Phen = 1,10-phenanthroline; [d] psa = 2-phenylsuccinate; [e] dms = 2,3-dimethylsuccinate; [f] btc = 1,3,5-benzenetricarboxylate; [g] BDC = 1,4-benzenedicarboxylate; [h] Not given; [i] L = 5-[2-{2,4,6-trioxotetrahydropyrimidin-5(2*H*)-ylidene}hydrazinyl]isophthalate; [j] TCA = tricarboxytriphenylamine; [k] The aldehyde employed is 2-nitrobenzaldehyde. [l] L-H_4 = 2,2'-diethoxy-1,1'-binaphthalene-6,6'-bisphosphonic acid. [m] L = 4,4′,4″-((2,4,6-trimethylbenzene-1,3,5-triyl)tris(methylene))tribenzoate; [n] L^{OMe} = 3,3′-((2,3,6,7-tetramethoxyanthracene-9,10-diyl)bis(4,1-phenylene))diacrylate.

20. References

(1) Bruker Apex2, B. A. I. Bruker Apex2, Bruker AXS Inc. Madison, Wisconsin, USA 2004.

(2) Sheldrick, G. M. SADABS. University of Gottingen: Gottingen, Germany 1996, p Program for Empirical Adsorption Correction.

(3) Sheldrick, G. M. A Short History of SHELX. *Acta Crystallogr. Sect. A Found. Crystallogr.* **2008**, *64* (1), 112–122. https://doi.org/10.1107/S0108767307043930.

(4) Sheldrick, G. M. Crystal Structure Refinement with SHELXL. *Acta Crystallogr. Sect. C Struct. Chem.* **2015**, *71*, 3–8. https://doi.org/10.1107/S2053229614024218.

(5) Farrugia, L. J. WinGX and ORTEP for Windows: An Update. *J. Appl. Crystallogr.* **2012**, *45* (4), 849–854. https://doi.org/10.1107/S0021889812029111.

(6) J. Rodríguez-Carvajal. FULLPROF 2000,Version 2.5d,. *FULLPROF 2000,version 2.5d, Laboratoire Léon Brillouin (CEA-CNRS), Centre d'Études de Saclay, Gif sur Yvette Cedex, France,*. 2000.

(7) Thavornpradit, S.; Killough, J. M.; Bergbreiter, D. E. Minimizing Solvent Waste in Catalytic Reactions in Highly Recyclable Hydrocarbon Solvents. *Org. Biomol. Chem.* **2020**, *18* (22), 4248–4256. https://doi.org/10.1039/d0ob00734j.

(8) Zhu, C.; Tang, H.; Yang, K.; Wu, X.; Luo, Y.; Wang, J.; Li, Y. A Urea-Containing Metal-Organic Framework as a Multifunctional Heterogeneous Hydrogen Bond-Donating Catalyst. *Catal. Commun.* **2020**, *135*, 105837. https://doi.org/10.1016/j.catcom.2019.105837.

(9) Wang, W.; Luo, M.; Yao, W.; Ma, M.; Pullarkat, S. A.; Xu, L.; Leung, P. H. Catalyst-Free and Solvent-Free Cyanosilylation and Knoevenagel Condensation of Aldehydes. *ACS Sustain. Chem. Eng.* **2019**, *7* (1), 1718–1722. https://doi.org/10.1021/acssuschemeng.8b05486.

(10) North, M.; Omedes-Pujol, M.; Young, C. Kinetics and Mechanism of the Racemic Addition of Trimethylsilyl Cyanide to Aldehydes Catalysed by Lewis Bases. *Org. Biomol. Chem.* **2012**, *10* (21), 4289–4298. https://doi.org/10.1039/c2ob25188d.

(11) Gu, J. Z.; Wan, S. M.; Kirillova, M. V.; Kirillov, A. M. H-Bonded and Metal(Ii)-Organic Architectures Assembled from an Unexplored Aromatic Tricarboxylic Acid: Structural Variety and Functional Properties. *Dalt. Trans.* **2020**, *49* (21), 7197–7209. https://doi.org/10.1039/d0dt01261k.

(12) Wu, W. B.; Zeng, X. P.; Zhou, J. Carbonyl-Stabilized Phosphorus Ylide as an Organocatalyst for Cyanosilylation Reactions Using TMSCN. *ACS Appl. Mater. Interfaces* **2020**, *85,* 14342–14350. https://doi.org/10.1021/acs.joc.9b03347.

(13) Zhang, Z.; Chen, J.; Bao, Z.; Chang, G.; Xing, H.; Ren, Q. Insight into the Catalytic Properties and Applications of Metal-Organic Frameworks in the Cyanosilylation of Aldehydes. *RSC Adv.* **2015**, *5* (97), 79355–79360. https://doi.org/10.1039/c5ra13102b.

(14) Zhang, Z.; Chen, J.; Bao, Z.; Chang, G.; Xing, H.; Ren, Q. Insight into the Catalytic Properties and Applications of Metal-Organic Frameworks in the Cyanosilylation of Aldehydes. *RSC Adv.* **2015**, *5* (97), 79355–79360. https://doi.org/10.1039/c5ra13102b.

(15) Sharma, M. K.; Singh, D.; Mahawar, P.; Yadav, R.; Nagendran, S. Catalytic Cyanosilylation Using Germylene Stabilized Platinum(Ii) Dicyanide. *Dalt. Trans.* **2018**,

47 (17), 5943–5947. https://doi.org/10.1039/c8dt00043c.

(16) Wang, W.; Luo, M.; Li, J.; Pullarkat, S. A.; Ma, M. Low-Valent Magnesium(i)-Catalyzed Cyanosilylation of Ketones. *Chem. Commun.* **2018**, *54* (24), 3042–3044. https://doi.org/10.1039/c8cc00826d.

(17) Harinath, A.; Bhattacharjee, J.; Nayek, H. P.; Panda, T. K. Alkali Metal Complexes as Efficient Catalysts for Hydroboration and Cyanosilylation of Carbonyl Compounds. *Dalt. Trans.* **2018**, *47* (36), 12613–12622. https://doi.org/10.1039/c8dt02032a.

(18) Sakai, T.; Miyata, K.; Tsuboi, S.; Takeda, A.; Utaka, M.; Torii, S. A Convenient Reductive Removal of Benzylic Hydroxyl and Trimethylsilyloxyl Groups with Me3SiCl-NaI-MeCN Reagent. *Bull. Chem. Soc. Jpn.* **1989**, *62* (11), 3537–3541. https://doi.org/10.1246/bcsj.62.3537.

(19) Strappaveccia, G.; Lanari, D.; Gelman, D.; Pizzo, F.; Rosati, O.; Curini, M.; Vaccaro, L. Efficient Synthesis of Cyanohydrin Trimethylsilyl Ethers via 1,2-Chemoselective Cyanosilylation of Carbonyls. *Green Chem.* **2013**, *15* (1), 199–204. https://doi.org/10.1039/c2gc36442e.

(20) Garnes-Portolés, F.; Rivero-Crespo, M. Á.; Leyva-Pérez, A. Nanoceria as a Recyclable Catalyst/Support for the Cyanosilylation of Ketones and Alcohol Oxidation in Cascade. *J. Catal.* **2020**, *392*, 21–28. https://doi.org/10.1016/j.jcat.2020.09.032.

(21) Garnes-Portolés, F.; Rivero-Crespo, M. Á.; Leyva-Pérez, A. Nanoceria as a Recyclable Catalyst/Support for the Cyanosilylation of Ketones and Alcohol Oxidation in Cascade. *J. Catal.* **2020**, *392*, 21–28. https://doi.org/10.1016/j.jcat.2020.09.032.

(22) Song, J. J.; Gallou, F.; Reeves, J. T.; Tan, Z.; Yee, N. K.; Senanayake, C. H. Activation of TMSCN by N-Heterocyclic Carbenes for Facile Cyanosilylation of Carbonyl Compounds. *J. Org. Chem.* **2006**, *71* (3), 1273–1276. https://doi.org/10.1021/jo052206u.

(23) Kolocouris, A.; Koch, A.; Kleinpeter, E.; Stylianakis, I. 2-Substituted and 2,2-Disubstituted Adamantane Derivatives as Models for Studying Substituent Chemical Shifts and C-Hax···Yax Cyclohexane Contacts - Results from Experimental and Theoretical NMR Spectroscopic Chemical Shifts and DFT Structures. *Tetrahedron* **2015**, *71* (16), 2463–2481. https://doi.org/10.1016/j.tet.2015.01.044.

(24) Jia, Y.; Zhao, S.; Song, Y. F. The Application of Spontaneous Flocculation for the Preparation of Lanthanide-Containing Polyoxometalates Intercalated Layered Double Hydroxides: Highly Efficient Heterogeneous Catalysts for Cyanosilylation. *Appl. Catal. A Gen.* **2014**, *487*, 172–180. https://doi.org/10.1016/j.apcata.2014.09.005.

(25) Batista, P. K.; Alves, D. J. M.; Rodrigues, M. O.; De Sá, G. F.; Junior, S. A.; Vale, J. A. Tuning the Catalytic Activity of Lanthanide-Organic Framework for the Cyanosilylation of Aldehydes. *J. Mol. Catal. A Chem.* **2013**, *379*, 68–71. https://doi.org/10.1016/j.molcata.2013.07.016.

(26) Dvries, R. F.; De La Peña-Oshea, V. A.; Snejko, N.; Iglesias, M.; Gutiérrez-Puebla, E.; Monge, M. Á. Insight into the Correlation between Net Topology and Ligand Coordination Mode in New Lanthanide MOFs Heterogeneous Catalysts: A Theoretical and Experimental Approach. *Cryst. Growth Des.* **2012**, *12* (11), 5535–5545. https://doi.org/10.1021/cg301096d.

(27) Dvries, R. F.; Iglesias, M.; Snejko, N.; Gutiérrez-Puebla, E.; Monge, M. A. Lanthanide Metal-Organic Frameworks: Searching for Efficient Solvent-Free Catalysts. *Inorg. Chem.* **2012**, *51* (21), 11349–11355. https://doi.org/10.1021/ic300816r.

(28) Dvries, R. F.; Snejko, N.; Iglesias, M.; Gutiérrez-Puebla, E.; Monge, M. A. Ln-MOF Pseudo-Merohedral Twinned Crystalline Family as Solvent-Free Heterogeneous Catalysts. *Cryst. Growth Des.* **2014**, *14* (5), 2516–2521. https://doi.org/10.1021/cg5002336.

(29) Gómez, G. E.; Kaczmarek, A. M.; Van Deun, R.; Brusau, E. V.; Narda, G. E.; Vega, D.; Iglesias, M.; Gutierrez-Puebla, E.; Monge, M. Á. Photoluminescence, Unconventional-Range Temperature Sensing, and Efficient Catalytic Activities of Lanthanide Metal-Organic Frameworks. *Eur. J. Inorg. Chem.* **2016**, *2016* (10), 1577–1588. https://doi.org/10.1002/ejic.201501402.

(30) Gómez, G. E.; Brusau, E. V.; Sacanell, J.; Soler Illia, G. J. A. A.; Narda, G. E. Insight into the Metal Content-Structure-Property Relationship in Lanthanide Metal-Organic Frameworks: Optical Studies, Magnetism, and Catalytic Performance. *Eur. J. Inorg. Chem.* **2018**, *2018* (20–21), 2452–2460. https://doi.org/10.1002/ejic.201701474.

(31) Gustafsson, M.; Bartoszewicz, A.; Martiín-Matute, B.; Sun, J.; Grins, J.; Zhao, T.; Li, Z.; Zhu, G.; Zou, X. A Family of Highly Stable Lanthanide Metal-Organic Frameworks: Structural Evolution and Catalytic Activity. *Chem. Mater.* **2010**, *22* (11), 3316–3322. https://doi.org/10.1021/cm100503q.

(32) He, H.; Ma, H.; Sun, D.; Zhang, L.; Wang, R.; Sun, D. Porous Lanthanide-Organic Frameworks: Control over Interpenetration, Gas Adsorption, and Catalyst Properties. *Cryst. Growth Des.* **2013**, *13* (7), 3154–3161. https://doi.org/10.1021/cg400531j.

(33) Karmakar, A.; Rúbio, G. M. D. M.; Paul, A.; Guedes da Silva, M. F. C.; Mahmudov, K. T.; Guseinov, F. I.; Carabineiro, S. A. C.; Pombeiro, A. J. L. Lanthanide Metal Organic Frameworks Based on Dicarboxyl-Functionalized Arylhydrazone of Barbituric Acid: Syntheses, Structures, Luminescence and Catalytic Cyanosilylation of Aldehydes. *Dalt. Trans.* **2017**, *46* (26), 8649–8657. https://doi.org/10.1039/c7dt01056g.

(34) Wu, P.; Wang, J.; Li, Y.; He, C.; Xie, Z.; Duan, C. Luminescent Sensing and Catalytic Performances of a Multifunctional Lanthanide-Organic Framework Comprising a Triphenylamine Moiety. *Adv. Funct. Mater.* **2011**, *21* (14), 2788–2794. https://doi.org/10.1002/adfm.201100115.

(35) Evans, O. R.; Ngo, H. L.; Lin, W. Chiral Porous Solids Based on Lamellar Lanthanide Phosphonates. *J. Am. Chem. Soc.* **2001**, *123* (42), 10395–10396. https://doi.org/10.1021/ja0163772.

(36) Wang, X.; Zhang, L.; Yang, J.; Liu, F.; Dai, F.; Wang, R.; Sun, D. Lanthanide Metal-Organic Frameworks Containing a Novel Flexible Ligand for Luminescence Sensing of Small Organic Molecules and Selective Adsorption. *J. Mater. Chem. A* **2015**, *3* (24), 12777–12785. https://doi.org/10.1039/c5ta00061k.

(37) Liu, X.; Lin, H.; Xiao, Z.; Fan, W.; Huang, A.; Wang, R.; Zhang, L.; Sun, D. Multifunctional Lanthanide–Organic Frameworks for Fluorescent Sensing, Gas Separation and Catalysis. **2016**, *45*, 3743–3749. https://doi.org/10.1039/c5dt04339e.

(38) An, H.; Wang, L.; Hu, Y.; Fei, F. Temperature-Induced Racemic Compounds and Chiral Conglomerates Based on Polyoxometalates and Lanthanides: Syntheses, Structures and Catalytic Properties. *CrystEngComm* **2015**, *17* (7), 1531–1540. https://doi.org/10.1039/c4ce01802h.

(39) Fei, F.; An, H.; Meng, C.; Wang, L.; Wang, H. Lanthanide-Supported Molybdenum-Vanadium Oxide Clusters: Syntheses, Structures and Catalytic Properties. **2015**, 18796–18805. https://doi.org/10.1039/c4ra16237d.